Observational test of a double reionization scenario by detecting galaxies at very high z with the GTC

Master Thesis

Cristina Cabello González

Supervised by:

Jesús Gallego Maestro & Nicolás Cardiel López

Universidad Complutense de Madrid

Facultad de Ciencias Físicas

September 2017

Abstract

One of the AMIGA (*Analytical Model for IGM and GAlaxy evolution*) predictions is that the reionization of the intergalactic neutral hydrogen occurred in two stages: a first one at z $\sim$ 10, due to Pop. III stars, and a second and definitive one at z $\sim$ 6, due to young galaxies formed at z $>$ 6. The study of high redshift galaxies is crucial for understanding this process, the formation and evolution of galaxies and the large scale structure in the Universe. The main goal of this project is to detect and quantify the predicted double reionization and the corresponding population of LAES (Luminous Lyman-α Emitters) at z $\sim$10. We want to detect LAEs at z=9.3 by the flux excess due to the Lyα emission and for this we have carried out the data reduction of a large amount of infrared images. A total of 16 objects have been identified from an ultra deep exposure (equivalent to a total of 4.6 h of integration) taken with a narrow band filter (with FWHM = 11nm and central wavelength λ_c = 1,254 μm) and the CIRCE nIR camera for GTC, but for the time being, no unidentified object already. The ultra deep image has been obtained within the Extended Groth Strip (EGS) field and the limit magnitude of this study has been $m_{F125W} \sim 22.3$.

Acknowledgements

I thank J.Gallego and N.Cardiel for giving me the opportunity to participate in this exciting project, for having taught me so much (and continue to do so), always with immense kindness and patience. Thanks for trusting me. To my family, because without their support would not be here today. To my friends, who share with me so many important moments. Thank you for joining me on the road and showing me what's really important in life, the things that are worth it. To those people who were once a part of my life and have given me the strength and the courage to continue and never give up.
To all who have believed in me, thank you.

There are no limits, because if you strive, with passion and work, dreams come true.

Index

1 Introduction **1**
1.1 The reionization of the Universe . . . 1
1.2 Overview of our project . . . 2
1.3 CIRCE . . . 3
1.4 The Extended Groth Strip, AEGIS-16 and 3D-HST . . . 4

2 Data reduction **5**
2.1 Data: the Observing Blocks . . . 5
2.2 Methodology . . . 6

3 Results **11**
3.1 Offsets calculation . . . 11
3.2 Seeing . . . 12
3.3 Dithering patterns . . . 13
3.4 Final image . . . 14
3.5 List of candidates . . . 17
3.6 Overall scientific analysis . . . 21

4 Conclusions **23**

5 Future work **24**

References **25**

6 Appendix **26**
6.1 Programming code . . . 26

List of Figures **39**

List of Tables **40**

Chapter 1

Introduction

1.1 The reionization of the Universe

The reionization of the matter happened after the Dark Ages of the cosmology and is the second of two major phase transitions of gas in the universe (after recombination). Reionization usually refers to the reionization of hydrogen gas although the primordial helium experienced the same process, but at different moment (helium reionization).
The universe was opaque before the recombination ($z \sim 1100$), but it became increasingly transparent as more electrons and protons combined to form neutral hydrogen atoms. It stayed neutral until the first objects in the universe started emitting light and energy which reionized the surrounding IGM. It is expected that quasars and first generations stars and galaxies were the main sources of energy that produced the reionization of the Universe.

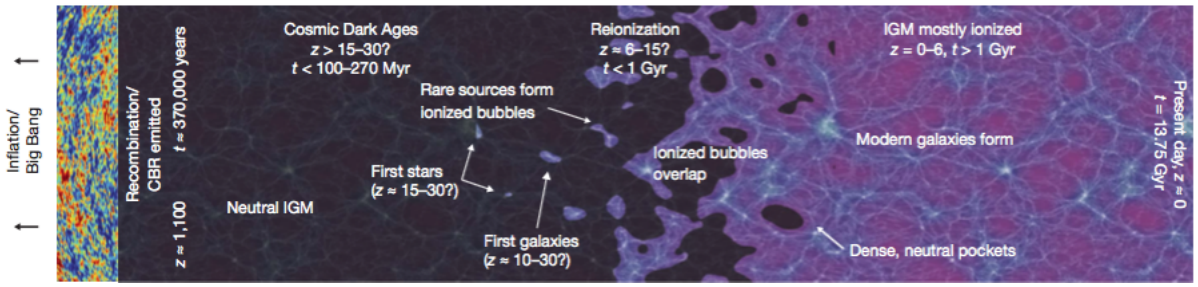

Figure 1.1: Cosmic history. In this figure we can see different phases of the Universe, since the Big Bang until the present time. We focused on the epoch of reionization, when the first stars and galaxies began to ionize the intergalactic medium (Brant E. Robertson et al, 2010. [6]).

The degree of ionization of hydrogen affects the efficiency with which the gas between a source and us absorbs the radiation that it emits at certain wavelengths (such as the Lyα transition). If the fraction of ionized hydrogen is high, the radiation is transmitted more easily. However, if most part of the hydrogen is neutral, we will observe many absorptions due to the IGM.
Due to the expansion of the Universe, these absorption lines are displaced to the red. The displacement increases with the distance between the source and the observer, so the absorptions present in different parts of the spectrum are produced by gas intercepted at different distances. Examining the spectrum of a quasar gives us not only spatial information, but also temporal information regarding the ionization of the universe. In the spectra of the quasars at z $<$ 6 we can see barely absorptions, because the hydrogen of the intergalactic medium is ionized, however in the spectra of the quasars at z $>$ 6 we observe the Lyman-alpha forest, produced by the radiation passing through regions of neutral gas, or the Gunn-Peterson through, due to the big accumulation of neutral hydrogen which produces that wavelengths less than Lyman limit (λ= 912 Å) are not transmitted. With this, we can estimate that the reionization started around z $\sim$ 10 and finished over z $\sim$ 6.
The anisotropy of the cosmic microwave background on different angular scales can also be used to study the reionization stage of the universe. For this task, we use the results of the satellites WMAP and Plank. Furthermore, the the 21 cm hydrogen line could give us more information about the early structures that formed.

One of the most distant galaxies are the Lyman Alpha Emitters (LAEs). These galaxies have typically low mass (10^8 - 10^{10} $M_\odot$) and they are relatively free of dust. Since LAEs are found at very high z, their detection is key to determinate the epoch of reionization. Usually, these galaxies are selected by narrow-band techniques due to an excess of their narrow-band flux at a wavelength which may be interpreted as their redshift:

$$\lambda = 1215.67\text{Å} \cdot (1 + z) \tag{1.1}$$

where z is the redshift, λ is the observed wavelength, and 1215.67 Å is the rest wavelength of the Lyman-α emission. Using the equation 1.1, we know that a source that emits photons Lyα at z= 9.3, it will be observed at present at λ= 1.25 μm. Therefore, we need a nIR camera to detect these type of galaxies at very high redshift.

1.2 Overview of our project

The ALBA team is actively following two parallel efforts: (1) the observational detection of high-z LAEs, and (2) An *Analytic Model of Intergalactic-medium and GAlaxy* (AMIGA) evolution since the dark ages previous to reionization. Although Planck mission in 2014 predicted one single re-ionization at z=11.3 ± 1.1, AMIGA predictions are that it is very likely that the reionization occurred in two stages: a first one at z ∼ 10 due to Pop. III stars, whose formation ended at this epoch as molecular cooling was quenched, and a second and definitive one at z ∼ 6, due to young galaxies formed at z > 6 (See Figure 1.2).
We search LAEs at z ∼ 9.3 in order to find observational proofs to confirm or not this scenario. Combining all the data we will obtain an ultra deep NB image. Comparison with J band fluxes allow us to select those targets with a flux excess in the Narrow-Band filter with respect to the Broad-band filter. If the target is at z= 9.3, it will be a dropout in all photometric bands bluer than J. Once we have rejected lower-z contaminants, accurate photometry in the NB filter will provide us with the Lyα luminosity and equivalent width. Number densities of LAEs will be compared with theoretical predictions to confirm or reject the double reionization scenario.

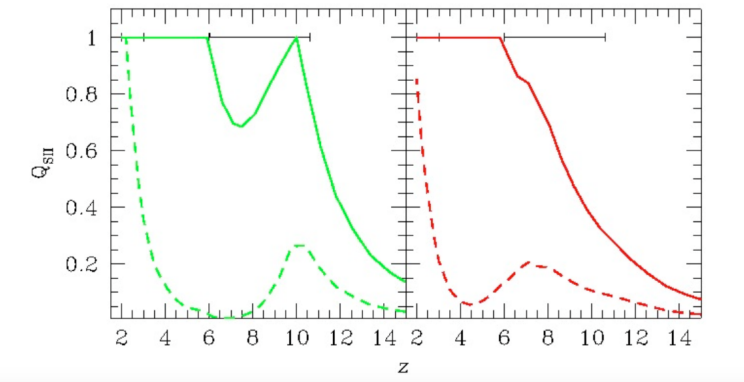

Figure 1.2: Evolution with redshift of the ionized hydrogen fraction (cont lines) and double ionized helium fraction (dashed lines) in the single reionization scenario (right panel) and in the double reionization scenario (left panel) as predicted by AMIGA model (Salvador-Solé 2015 Ref: [8]). AMIGA was tuned to reproduce the z < 6 universe. Universe fully ionized Q_{SII}=1, and neutral Q_{SII}=0

In this project we have the opportunity to use the largest optical telescope on the world to observe the most distant galaxies. Our main aims are:

- Carry out the data reduction of 23h exposure with the CIRCE nIR camera for GTC.
- Detect the population of LAEs at z=9.3 by the flux excess due to the Lyα emission in a NB filter.
- Analyse the results and the hypothetical scenario of double reionization of the Universe.

This work is a pilot project to know the limit magnitude that we can achieve with 5h of exposure time with CIRCE and thus to estimate if we will able to detect LAEs in a future study.

1.3 CIRCE

The Canarias InfraRed Camera Experiment (CIRCE) is a near-infrared camera designed and constructed by the University of Florida, to be used as a visitor instrument at GTC. The detector is a 2048 x 2048 pixels engineering grade HAWAII-2RG optimized to work on the 1-2.5 micron wavelengths range. It covers a 3.4' x 3.4' field of view with plate scale of 0.1"/pix and it is subdivided into 32 independent channels for quick readout (2 channels are inactive). The CIRCE system gain is 5.3 ± 0.5 e-/ADU and the read noise is ∼ 30-45 e- RMS (channel dependent). The dark current is essentially negligible.
NIR detectors have many more cosmetic defects than their optical CCD counterparts, and this detector is not an exception (See Figure 1.3 Left). Nevertheless, CIRCE has characteristics that complement those of EMIR so that the instrument is expected to remain competitive for a long time. These key capabilities include: high-resolution (< 0.3 arcsec) seeing-limited imaging, narrow-band imaging, high time-resolution (<10 Hz) photometry and linear polarimetry (Ref: [18] and [19]).

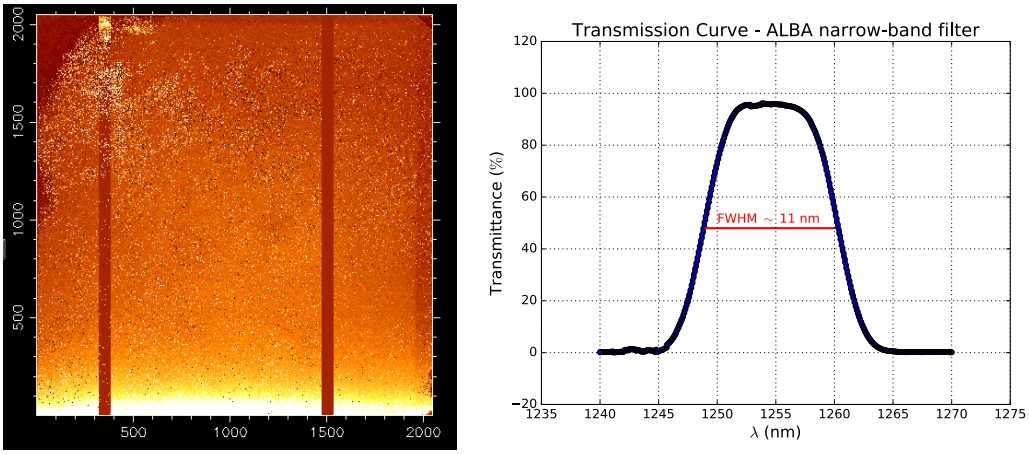

Figure 1.3: Left:Raw image taken with CIRCE. This figure shows the poor cosmetic of the detector: the upper left corner is not useful, there are many defective pixels, and two non functional channels. Right: Transmission curve of ALBA narrow-band filter. The profile has central wavelenght $\lambda_c = 1,254\mu m$ and FWHM = 11 nm. The curve has been measured at ambient temperature.

For this project we use the ALBA narrow-band filter in the near IR with FWHM = 11nm and central wavelength λ_c= 1,254 μm. The transmittance curve is shown in Figure 1.3 (Right). The filter has been selected to coincide with a region which avoids OH emissions and atmosphere absorptions and lies in a wavelength range with minimum sky continuum emission, leading to discrete redshift values.

As we are working in the infrared, we employ a standard dithering (shift+coadd) technique to improve image quality and resolution. By combining multiple images of a target at slightly different positions on the detector, one can compensate for detector artefacts (blemishes, dead pixels, hot pixels, transient bad pixels, and plate-scale irregularities) that may not be completely corrected by application of the calibration reference files. Combining images, whether dithered or not, can also remove any residual cosmic ray flux that has not been well removed. Substantially shorter exposure times are generally needed to allow dithering on timescales sufficient to properly subtract the rapidly-varying NIR sky background.
One can define the number of ramps and the time of exposure of each ramp to get the best results in the observation strategy. Readout mode: the detector is first cleared and then readout twice in Correlated Double Sampling (CDS) mode. First read (Rd1) occurs at the start and second read (Rd2) at the end of the exposure (See Figure 1.4). Each read is an extension of the FITS files, and the difference Rd2-Rd1 is the science signal.

Darks and flat fields are required for the calibration of CIRCE images. The dark frames are used primarily to subtract the electronic offsets of the detector (since the dark current is too small). The electronic offsets have significant structure, and depend on the exposure time and number of reads. Flat fields are used to correct the pixel-to-pixel response of the instrument to light. It is necessary to use flat fields because for an engineering-grade array such as the on used in CIRCE, these variations are significant and science-quality analysis requires the use of flat fields.

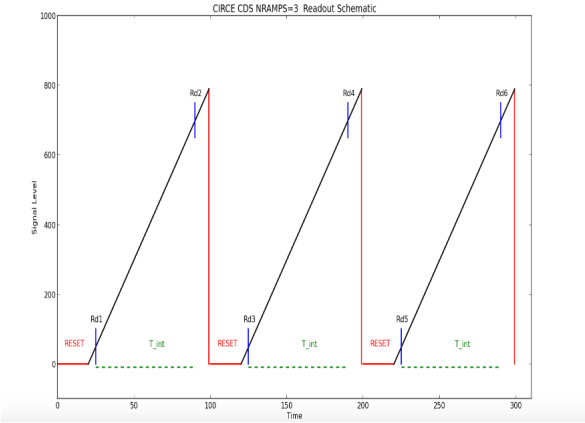

Figure 1.4: Readout mode with 6 reads and 3 ramps. Collapsing the 3 science images we obtain an individual image with more exposure time. (Ref: [19])

1.4 The Extended Groth Strip, AEGIS-16 and 3D-HST

The Extended Groth Strip (EGS) is a small region (70 × 10 arcmin) between the constellations of Ursa Major and Boötes. It has been observed by HST and it is estimated that there are at least 50.000 galaxies in this field. A survey termed All-wavelength Extended Groth Strip International Survey (AEGIS) utilized four orbiting telescopes and four ground-based telescopes to study the EGS. AEGIS-16 is a region in the EGS, with field of view 123 x 136 arcsec approximately and coordinates RA: 14 h 20 m 0 s and DEC: +52° 55' 0". Our study is focussed just there in order to search for Lyα emitters. In Figure 1.5 (Right) we observe a color mosaic of a piece of EGS where our field of view is marked with a blue rectangle.
3D-HST is a near-infrared spectroscopic survey with the Hubble Space Telescope designed to study the physical processes that shape galaxies in the distant Universe. It covers $\sim$ 600 square arcminutes of well-studied extragalactic survey fields (AEGIS, COSMOS, GOODS-S, UKIDSS-UDS) with two orbits of primary WFC3/G141 grism coverage and two to four orbits with ACS/G800L coverage. The images obtained in this survey are deeper than most ground-based observations. Furthermore, 3D-HST provides information of a sample of $\sim$ 10.000 galaxies at redshifts z>1 (Ref: [14]). Tiles of observations by HST in the field AEGIS are shown in Figure 1.5 (Left).

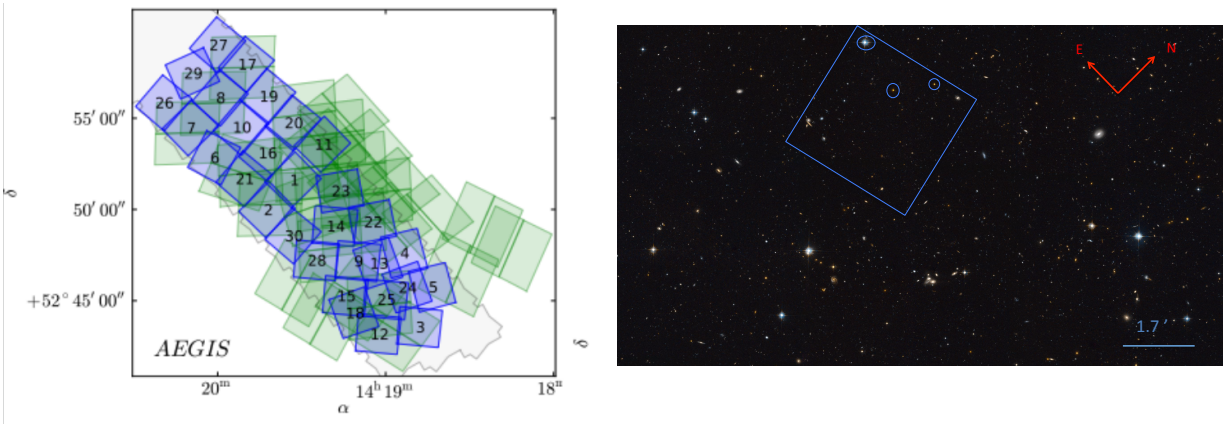

Figure 1.5: Left: Layout of the 30 3D-HST pointings in the extragalactic field AEGIS. Primary WFC3 F140W+G141 pointings are shown in blue with the pointing ID numbers as defined in the HST Phase II file. The locations of the parallel ACS F814W+G800L observations are shown in light green. The light gray polygons indicate the footprint of the CANDELS WFC3 imaging, including both the "wide" and "deep" components of that survey (Ref: [14]). Right: Color mosaic of AEGIS-16. The image shows a piece of The Extended Groth Strip (EGS) based on the results of a series of observations by the Hubble Space Telescope (ACS). The blue rectangle indicates our Field-Of-View 204.8 x 204.8 arcsec (AEGIS-16 and a little piece of AEGIS-21) and the three blue circles show the stars of reference. Position : RA: 14h 19m 17.84s, DEC: 52° 49' 26.49". Orientation: North is 220.3° right of vertical. Filters: optical V band (555 nm) and pseudogreen V+I bands, Infrared I band (814 nm). Release date: 6 March 2007, 19:00.

Chapter 2

Data reduction

2.1 Data: the Observing Blocks

In order to detect Lyman α emitters at z $\sim$ 9.3 we have carried out the data reduction of a large amount of infrared images taken with CIRCE. The data are divided in observing blocks (OB), and some information about them is shown in Table 2.1 (only the information of the first ten observing blocks is shown). The individual OBs have a total exposure time of 3300s, with 11 shifted images (with exception of OB0005). After OB0003, we changed the observing strategy and we began to perform 5 ramps instead of 3 in the readout mode of the detector.

TABLE *2.1:*
OB SUMMARY

OB (1)	**Dithering pattern** (2)	**Date** (3)	**Airmass** (4)	**Total exp. (s)** (5)
OB0001	3 ramps × 100 s × 11 frames	20/05/2016	1.11	3300
OB0002	3 ramps × 100 s × 11 frames	20/05/2016	1.10	3300
OB0003	3 ramps × 100 s × 11 frames	21/05/2016	1.13	3300
OB0004	5 ramps × 60 s × 11 frames	23/06/2016	1.10	3300
OB0005	5 ramps × 60 s × 12 frames	23/06/2016	1.13	3600
OB0006	5 ramps × 60 s × 11 frames	25/06/2016	1.10	3300
OB0007	5 ramps × 60 s × 11 frames	25/06/2016	1.14	3300
OB0008	5 ramps × 60 s × 11 frames	20/07/2016	1.23	3300
OB0009	5 ramps × 60 s × 11 frames	21/07/2016	1.29	3300
OB0010	5 ramps × 60 s × 11 frames	22/07/2016	1.21	3300

NOTES: Col(1): Observing Blocks. Col(2): Dithering pattern; number of ramps (the number of times to repeat the readout scheme selected), exposure time in each ramp in seconds, and number of exposures (number of offsets positions). Col(3): Observation date dd/mm/yyyy. Col(4): Mean airmass between initial and final airmass. Col(5): Total exposure time in seconds.

Besides this information, headers provide us the position of each image for all the observing blocks. The first ten dithering patterns are shown in Figure 2.1. According to the information of the headers, only OB0006 and OB0008 have different dithering pattern while OB0009 is considerably shifted. Anyway, we are going to calculate the offsets by ourselves, thus we make sure we are correcting the real displacements just in case the information of the header is not quite correct. We start the data reduction working with the first ten observing blocks, but later we will focus on a few of them.

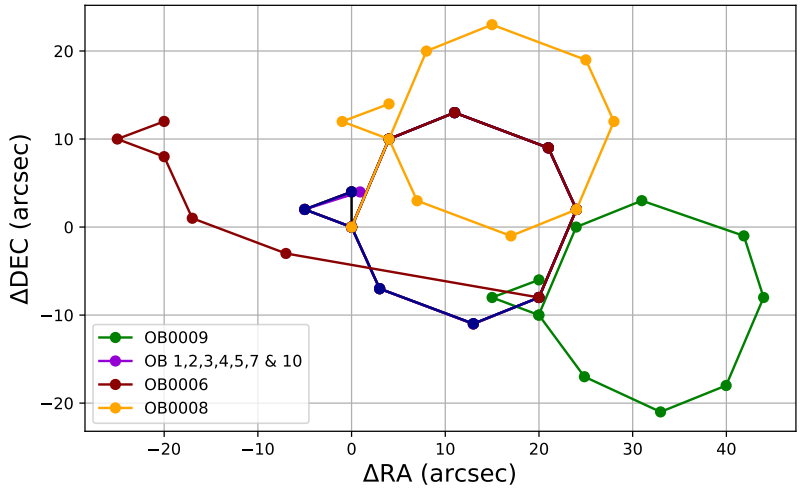

Figure 2.1: Dithering patterns of the first 10 observing blocks obtained from the information of the headers. Note that OB0001, OB0002, OB0003, OB0004, OB0005, OB0007, and OB0010 are taken in the same coordinates.

2.2 Methodology

The first step is to take the raw images and to collapse their ramps to obtain the coadded images (each of them with 300 seconds of exposure time). Furthermore, we use the list of darks[1] (with the same exposure time) and compute an average dark[2]. We subtract consecutive coadded images to remove some dead pixels of the detector (many of them should be in the same position in all the images)[3]. The new images show more clearly two objects: a bright star and a faint star (See Figure 2.2).

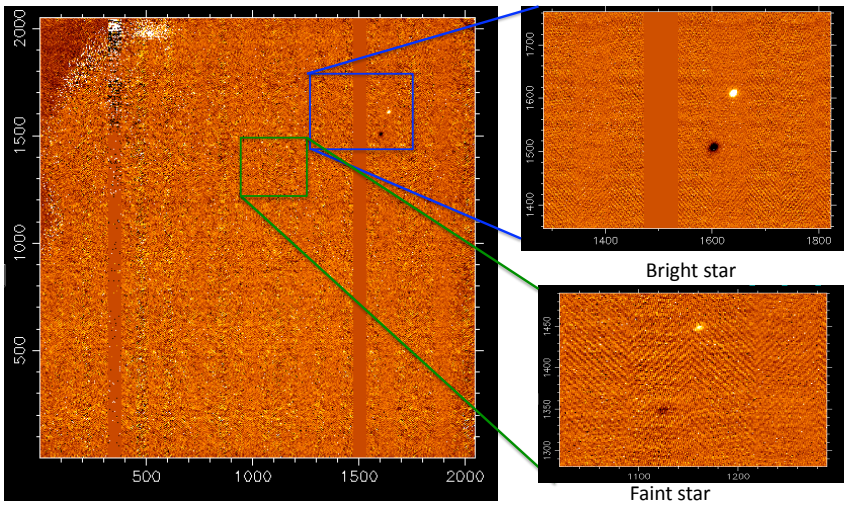

Figure 2.2: OB0001: image coadded 1 minus image coadded 2. We have done zoom in the detector image to measure the offsets between both images. The same star appears in positive and negative due to the subtraction of two shifted images.

The next step is the measurement of the offsets between images in each observing block, that is to say, to obtain the dithering pattern.

[1]Previously we performed a statistical analysis of the darks to ensure that there were not defective images.
[2]This task is carried out with the script *"reduce.py"* in Python (See Appendix 6.1).
[3]We perform this task with the script *"generate_consecutive_subtracted.py"* (See Appendix 6.1)

2.2.1 Offsets selection

For the determination of offsets we have performed several processes in order to obtain the most accurate measures. In the coadded subtracted images we count with two reference objects : a bright star and a faint star. With the coordinates of these objects we can calculate the offsets between each image (and so obtain the dithering pattern) and between observing blocks too. First, for both the bright star and the faint star we have measured the coordinates with the cursor at the brightest point. Second, we have performed an adjustment of the centroid. Both methods provide similar results. Moreover with the gaussian fit we obtain the FWHM that allow us to calculate the seeing (See Figure 2.3 Right). All of this was performed with *xnirspec* (See Figure 2.3 Left). The results are shown in Table 3.1 and Table 3.2.

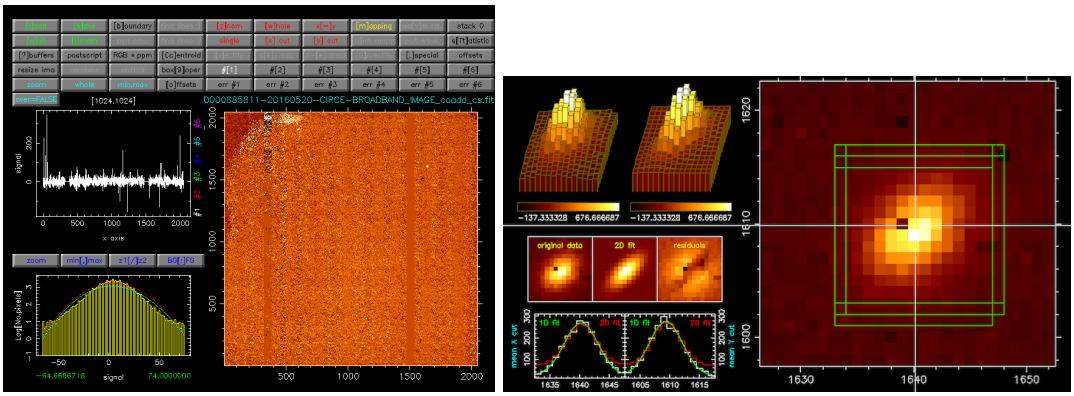

Figure 2.3: Left: The interface xnirspec. This programs has been employed to perform basic image manipulations, filtering, and the manual determination of the offsets between images. Right: Centroid fitting. With xnirspec we can perform a fit of the centroid and obtain the FWHM that allow us to calculate the seeing. In this case, despite of having a dead pixel in zone of the star, we achieve a reasonable fit.

This provides us a list of offsets between frames. Finally we apply the technique of cross-correlation to refine these offsets[4](See Figure 2.4). We carry out this method in a window of 41 x 41 pixels and it is repeated 49 times for each couple of images, where the region containing the star is slightly shifted following a grid pattern in order to obtain different estimates of the sought offset. The individual values are averaged and an estimation of the corresponding uncertainty obtained.

```
('0000885811-20160520-CIRCE-BROADBAND_IMAGE_coadd_cs.fits', 0, 0)
('0000885812-20160520-CIRCE-BROADBAND_IMAGE_coadd_cs.fits', 37, 103)
('0000885813-20160520-CIRCE-BROADBAND_IMAGE_coadd_cs.fits', 101, 134)
('0000885814-20160520-CIRCE-BROADBAND_IMAGE_coadd_cs.fits', 199, 94)
('0000885815-20160520-CIRCE-BROADBAND_IMAGE_coadd_cs.fits', 225, 24)
('0000885816-20160520-CIRCE-BROADBAND_IMAGE_coadd_cs.fits', 184, -77)
('0000885817-20160520-CIRCE-BROADBAND_IMAGE_coadd_cs.fits', 112, -108)
('0000885818-20160520-CIRCE-BROADBAND_IMAGE_coadd_cs.fits', 8, -66)
('0000885819-20160520-CIRCE-BROADBAND_IMAGE_coadd_cs.fits', -27, 5)
('0000885820-20160520-CIRCE-BROADBAND_IMAGE_coadd_cs.fits', -78, 25)
('0000885821-20160520-CIRCE-BROADBAND_IMAGE_coadd_cs.fits', -34, 46)
* Reference image: 0000885811-20160520-CIRCE-BROADBAND_IMAGE_coadd_cs.fits
* Offset image...: 0000885812-20160520-CIRCE-BROADBAND_IMAGE_coadd_cs.fits
>>> Offset (y, x): [-2.  0.]
>>> Error.......: 0.580558698277
>>> Diffphase....: 0.0

Press RETURN to continue...
```

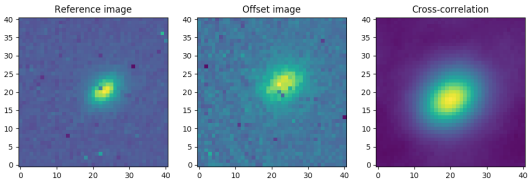

Figure 2.4: Applying the cross-correlation technique. In the console we see the name of reference image and shifted image, and the offsets obtained (x and y). With the plots we can check that the process is carried out properly.

For the bright star the error in the calculated offsets is always lower than 1 pixel but it should be noted that for the faint star this method does not work very well, so in general we use the refined data of the bright star except when this star is not visible (sometimes we could not measure offsets because the star appeared in the inactive channel of the detector), in that case we use the offset obtained with the faint star (before cross-correlation).
Now that we have the dithering pattern (with the refined offsets) for each observing block, we can compare these dithering patterns. Although the header information indicate that there are not offsets between observing blocks, we found that the dithering patterns are displaced. To generate the final image, we must apply these offsets too.

[4]For this process, we employ the script *"mide_offsets.py"* (See Appendix 6.1).

2.2.2 Offsets between ramps

At this point, we discovered something important. We appreciated that in the coadded images, the star of reference appeared a little elongated instead of exhibiting a round shape. We modified our code to obtain the individual ramps of each image. Then, we examined these ramps and we realized that in some cases the star showed a little displacement! (only 1 or 2 pixels between ramps). Initially we had collapsed the ramps because we thought that they were taken in the same place but it turned out that the telescope tracking was not accurate enough, so for each image (100s × 3 ramps = 300s) the star has been moving (See Figure 2.5). Once we realized this, we set about solving the problem. Only the three first observing blocks have three ramps of 100s, all the other observing blocks have five ramps of 60s to help us to correct the bad tracking.

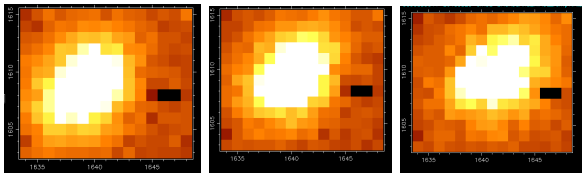

Figure 2.5: OB0001: Zoom around the bright star in the three individual ramps corresponding to the same image. The star appears elongated in the direction of the displacement.

We generated the subtracted ramps images (ramp 1 of image 1 minus ramp 1 of image 2, ramp 2 of image 1 minus ramp 2 of image 2 ...and so on) in order to measure the offsets between ramps in each image. Furthermore we improved the calculation of the offsets using the cross-correlation technique after performing a cleaning of defective pixels in the images. We did this with the program *"cleanest"* (See Figure 2.6) which is part of an astronomical data reduction package created by N. Cardiel, *REDUCEME* (Ref: [21]). This allowed us to interpolate the defective pixels with the values of the surrounding pixels. At the end we have spent a lot of time *cleaning up* a section of 100 × 100 pixels around the star of reference of each subtracted ramp to ensure that the reliability of the computed offsets.

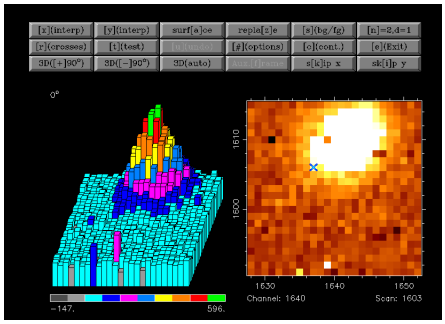

Figure 2.6: cleanest (REDUCEME) interface. With this program we can solve the problem of some dead pixels that carry weight in the cross-correlation technique. We interpolate those pixels with the values of the surrounding pixels in a section of 100 × 100 pixels around the center of the star of reference.

Now that we have the subtracted ramps images free of dead pixels around the star of reference we used the cross-correlation technique again to calculate the offsets between ramps for each image. Then, we corrected these displacements and align the ramps in order to generate a datacube. We computed the median image of the datacube formed by all the ramps[5] (this new image will replace the old coadded image). With these median images we achieved to reduce the number of bad pixels and to correct the elongated shape of the star of reference (See Figure 2.7). After correcting the offsets between ramps, the star of reference appears in the median images with a more rounded shape, and without so many dead pixels, so it is more easy to measure the seeing. We repeated the process of interpolation of defective pixels around the star of reference with the median images. It has taken us a long time inasmuch as there were many images for each OB and a large amount of bad pixels. After that, with the median images cleaned of defective pixels, we recalculated the offsets between images with the cross-correlation technique. The result is that the offsets did not vary more than 1-2 pixels in comparison with the offsets previously obtained, but in this way we make sure that we were calculating the reliable offsets. At this point, we generated a final list with the offsets between images, and we were ready to execute *imcombine*.

[5]We do this with the script *"median_of_ramps.py"* (See Appendix 6.1)

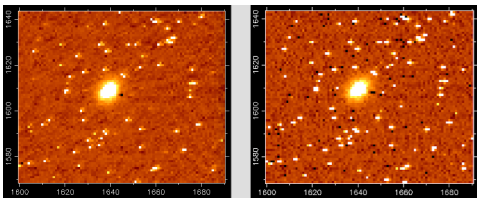

Figure 2.7: Comparison between the new image (median image) and the initial image (coadded image) of the image 1 (OB0001). Left: Median image of the datacube obtained after correct the offsets between the three ramps. Right: Coadded image obtained after the collapse of all ramps (without correcting offsets).

2.2.3 Imcombine

The program reads a file with the images, the dark of each one, and the offsets (with respect to the first image). Moreover we fed the program with a mask frame (defining the regions of the two inactive channels in pixels). We have repeated all the next steps in several iterations. In a first iteration a mask of objects is generated, and then it is employed in the following iterations to delete pixels with signal of objects during the flat field computation. The steps are the following:

(1) Normalize individual (raw-dark) frames.
Option 0: divide by median of full frame.
Option 1: divide by median of each quadrant (excluding cosmetic defects and objects).
Option 2: divide by smooth 2D sky fit.
We choose option 0.

(2) Compute superflat.
Previous images are combined (excluding only the objects). An image with the number of images/pixel are generated. A superflat image is generated with the mean of the useful images in each pixel.

(3) Compute individual (raw-dark) / superflat.
Previous (raw-dark) frames are divided by the superflat. The resulting images are used to obtain an average value (the median) of the sky (excluding cosmetic defects and objects).

(4) Sky subtraction in (raw-dark) / superflat.
Option 0: subtract median of each quadrant.
Option 1: subtract smooth 2D fit.
Option 2: subtract median of each 64 CIRCE regions.
We choose option 2.

(5) Combine sky-subtracted (raw-dark) / superflat frames.
Combination of all images is performed pixel to pixel. For each pixel, the histogram of the signal of the pixel in all individual frames is generated. A fraction of pixels in both sides of the histogram is removed. Mean and standard deviation of the histogram are calculated. Finally, mean and standard deviation are recalculated, removing pixels that are not compatible with a number of times the previous standard deviation in respect of the previous mean. In this step the final combined image is generated, image of errors (standard deviations) and image with the number of pixels employed in each pixel of the final image as well.

(6) Compute r.m.s. versus number of frames.
Using the final combined image and the image with the number of pixels employed in each pixel of the final image, the program calculates the standard deviation of all pixels generated with the same number of pixels and saves the result.

(7) Read r.m.s versus number of frames file, create: fake noise image and mask of objects.
A fake noise image is generated using the error of a unique image divided by the root square of the number of pixels employed in each pixel of the final image.
We increase the r.m.s. in the borders, and we define an useful rectangle in which Sextractor is executed to generate a mask of objects.

Flatfielding has been carried out using the own scientific images. When observing in the Infrared, the sky is really bright and the detector can easily saturate. For this reason, short exposures are taken. In these exposures bright objects can be detected. To obtain the flat field, all the shifted images are stacked (without correcting the offsets between them), so the objects will be in different locations (the dithering pattern). Doing the median of all the images we remove the objects, because they are small (a pixel can be very bright in one image, but not in all). This median image is uniform so we can use it as our flat field. If we had used

the mean instead of the median, the objects signal would not have been removed properly from the flatfield image. In principle, obtaining the median of all these images provides a reasonable flat field (also known as superflat) without the signature of the objects signal. However, since the median is noisier than the mean, and considering that each observing block contains a relatively small number of images, *imcombine* computes the mean and removes the objects iteratively. In particular, the mask of objects generated in the initial execution of *imcombine* is employed to remove the pixels affected by object signal when computing the superflat in subsequent executions of the program. In our case, we have generated the superflat with the mean of the useful images in each pixel (step 2 of *imcombine*), so the dithering pattern is observed in the superflat image. However, as we are using a mask of objects in the iteration 2, we have corrected this effect. In Figure 2.8 (Left) we can see the result of subtracting the superflat of iteration 2 from the superflat of iteration 1 for the OB0001.

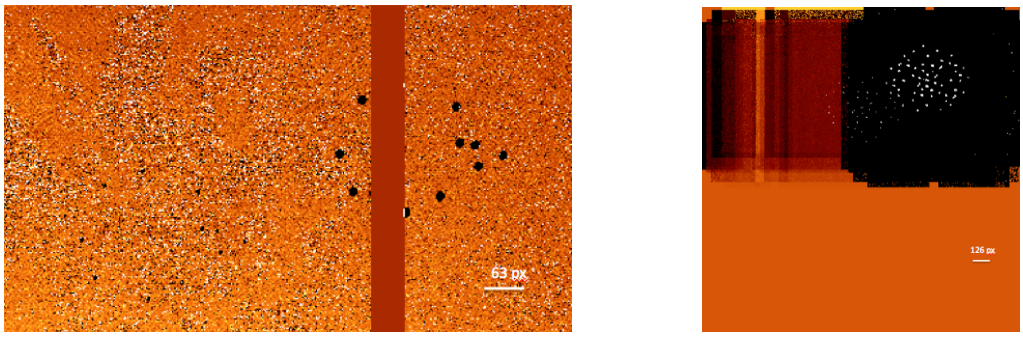

Figure 2.8: Left: A piece of the resulting image of the subtraction of the superflat of iteration 2 from the superflat of iteration 1 for the OB0001. Dithering pattern is shown for the bright and the faint star. This provide us the proof that with the mask of objects we are obtaining a good superflat. Right: Result of the subtraction of the combined images of iteration 2 from the combined image of iteration 1 for the OB0010. The pixels in the bottom half of the resulting image have a value of zero, but the top half of the image shows clear variations. The sky subtraction has been performed by the median of each quadrant. Orientation : North is 218° right of the vertical for both images.

We have also studied the influence of using different strategies when carrying out the sky subtraction. Initially we computed the median signal in each quadrant, but we realized it is not the best option because we did not remove totally the effect of the inactive channels. We subtracted the combined image of the iteration 1 to the combined image of iteration 2 (where we had applied a mask of objects in the steps of *imcombine*) (See Figure 2.8 Right) in order to compare the results of the two iterations (since at first glance they looked similar). The bottom of the image is flat (identical in both iterations), but the top of the image shows slight variations (around $\sim 10^{-4}$ counts). In particular, we observe two clouds of white dots. What is happening? In the step of sky subtraction, *imcombine* has computed the average value of each quadrant, so in the first iteration the sky average value is wrong because of the presence of the two objects relatively bright objects. In the second iteration (with the mask of objects) we have corrected this. Although the second iteration is better because we have used a mask of objects, our mask has few objects (and they are faint), and the cosmetic of the detector is really poor, so the effect is negligible in this case, but it is useful for us to understand how *imcombine* works and knowing that we are carrying out the data reduction in the best possible way. Finally, as we observed in the combined images some structures due to the inactive channels, we subtract the median of each 64 CIRCE regions in the sky subtraction in order to sort out this problem.

2.2.4 Combining OBs

We have five observing blocks completely reduced: OB0001, OB0002, OB0003, OB0004 and OB0010. The next step is to combine the reduced images to obtain a final deep image. We have used the IRAF astronomical software for this part. At first, we calculated the rotation of OB0010 with trigonometric relations (with the three objects that we observe in the reduced images), and we obtained a value of 3° counter-clock wise. The rotation has been corrected with the task *rotate*. We trimmed the images so that all of them have the same size (since the edges do not contain useful information). We used the task *ccdproc* for this (*imred.ccdred*). The command *imalign* allowed us to correct the offsets between images. With the images aligned, the last step was to combine them. We employed the task *imcombine* and finally we generated our deep image (See Figure 3.5 Right).

Chapter 3

Results

After the data reduction of the infrared images, we present the first results of the work in order to obtain an ultra deep image within EGS where we can identify objects and find candidates of Lyman α emitters. Possible candidates will give us relevant information about the beginning of the epoch of reionization.

3.1 Offsets calculation

We took the first image of the reduced observing blocks and we used *xnirspec* to calculate the position of the bright and the faint star of reference with two methods: with the cursor at the brightest point and performing an adjustment by centroid. Carrying out this for all images in each observing block we got the dithering pattern. In addition of this, comparing these coordinates we could obtain the offsets between observing blocks. These results are shown in Tables 3.1 and 3.2.

We see that the values of the offsets between OBs obtained for the bright and the faint star are in good agreement. In case of discrepancy, the results obtained for the bright star are always better, because it is easier to measure. The blank entries represent the cases where it has been impossible to perform a centroid adjustment (the gaussian fit is not good in all the images mainly due to bad pixels). We have to emphasize the difference between ΔDEC in OB0010 since in this case the results are quite different when we use the bright or the faint star to measure the offset. How can we explain this? Despite of the header's information does not indicate any rotation, after the data reduction (when we obtained an image with better quality and we can see more objects) we discovered that actually the images taken in OB0010 show a rotation of 3° counter-clock wise. We corrected the rotation before the combination.

TABLE *3.1:*
Brightest star's analysis : First image

OB	$\mathbf{X_{cursor}}$ **(pixels)**	$\mathbf{Y_{cursor}}$ **(pixels)**	$\mathbf{X_{centroid}}$ **(pixels)**	$\mathbf{Y_{centroid}}$ **(pixels)**	**ΔRA (arcsec)**	**ΔDEC (arcsec)**
(1)	**(2)**	**(3)**	**(4)**	**(5)**	**(6)**	**(7)**
OB0001	1639.96	1608.92	1640.34	1609.46	0.00	0.00
OB0002	1682.00	1609.07	-	-	4.20	0.02
OB0003	1672.72	1614.22	1672.42	1614.42	3.28	0.53
OB0004	1656.68	1509.03	-	-	1.67	−9.99
OB0005	1703.79	1510.76	1704.35	1510.74	6.38	−9.82
OB0006	1667.34	1587.82	1667.68	1587.70	2.74	−2.11
OB0007	1675.95	1600.05	-	-	3.60	−0.89
OB0008	1629.56	1626.22	1629.68	1626.48	−1.04	1.73
OB0009	1406.84	1723.03	1406.81	1723.11	−23.31	11.41
OB0010	1590.11	1663.75	1590.13	1663.99	−4.99	5.48

NOTES: Col(1): Observing Blocks. Col(2) and Col(3): Coordinates measured with the cursor at the brightest point. X and Y in pixels. Col(4) and Col(5): Coordinates measured by centroid. X and Y in pixels. Col(6): Right Ascension offsets regarding the first image of OB0001 in arcsec. Col(7): Declination offsets regarding the first image of OB0001 in arcsec.

TABLE *3.2:*
FAINT STAR'S ANALYSIS: FIRST IMAGE

OB	X_{cursor} (pixels)	Y_{cursor} (pixels)	$X_{centroid}$ (pixels)	$Y_{centroid}$ (pixels)	ΔRA (arcsec)	ΔDEC (arcsec)
(1)	(2)	(3)	(4)	(5)	(6)	(7)
OB0001	1161.04	1448.00	-	-	0.00	0.00
OB0002	1203.14	1447.05	-	-	4.21	−0.10
OB0003	1192.45	1454.15	1192.33	1454.09	3.14	0.62
OB0004	1177.98	1348.77	-	-	1.69	−9.92
OB0005	1224.05	1349.91	1223.79	1350.56	6.30	−9.81
OB0006	1187.86	1426.92	1187.54	1427.17	2.68	−2.11
OB0007	1196.28	1438.65	-	-	3.52	−0.94
OB0008	1151.44	1466.32	1151.69	1466.70	−0.96	1.83
OB0009	927.28	1564.77	927.73	1564.55	−23.38	11.68
OB0010	1120.22	1476.22	1120.21	1476.16	−4.08	2.82

NOTES: Col(1): Observing Blocks. Col(2) and Col(3): Coordinates measured with the cursor at the brightest point. X and Y in pixels. Col(4) and Col(5): Coordinates measured by centroid. X and Y in pixels. Col(6): Right Ascension offsets regarding the first image of OB0001 in arcsec. Col(7): Declination offsets regarding the first image of OB0001 in arcsec.

3.2 Seeing

To estimate seeing we have taken the values of σ_x and σ_y and we used the following expression:

$$Seeing('') = \sqrt{\sigma_x \cdot \sigma_y} \cdot 2.35 \cdot 0.1 \tag{3.1}$$

where 2.35 is the conversion factor and 0.1 "/pixel is the plate scale. We used the results of fitting a gaussian to the stars used in the previous section. Table 3.3 shows the results of the analysis of each image for five observing blocks. In principle, we think that the observational conditions were similar because the estimated seeing has not varied more than 10%.

TABLE *3.3:*
SEEING ESTIMATION (")

Image	Seeing (")				
	OB0001	OB0002	OB0003	OB0004	OB0010
(1)	(2)	(3)	(4)	(5)	(6)
1	0.49	0.59	0.58	0.54	0.51
2	0.56	0.47	0.38	0.62	0.52
3	-	0.61	0.66	0.45	-
4	0.48	0.74	0.69	0.60	0.63
5	0.42	0.62	0.62	0.60	0.54
6	0.63	-	-	-	0.60
7	-	0.58	-	0.52	0.57
8	0.49	0.57	0.64	0.60	0.54
9	0.62	0.61	0.60	0.57	0.54
10	0.56	0.67	0.57	0.59	0.37
11	0.61	0.56	0.54	0.57	0,62
Mean	0.54	0.60	0.58	0.57	0.55

NOTES: Col(1): Number of image. Col(2), Col(3), Col(4), Col(5) and Col(6): Seeing in arcsec for OB0001, OB0002, OB0003, OB0004 and OB0010 respectively. The blank entries represent the cases where it has been impossible to perform a centroid adjustment (the gaussian fit is not good or the star was in the inactive channel or very close to it)

3.3 Dithering patterns

The error in our offsets is always lower than 1 pixel, i.e. 0.1 arcsec, so the error bars are tiny in the Figures 3.1, 3.2 and 3.3. We measured the offsets using the faint star as well, but the cross-correlation technique does not work well in this case. It is better to use the offsets measured by us in a manual way using *xnirspec*.

3.3.1 OB0001

We have measured the seeing in the median images, and we have the offsets between each image of OB0001 (See Table 3.4). Graphical representation of dithering pattern is shown in Figure 3.1, where we can observe the difference between the header's information and the real offsets.
In red the coordinates obtained from the information of the header, and in blue the coordinates measured by us with the bright star, and refined using the cross-correlation technique. This proves that we can not trust the information of the headers.

TABLE *3.4:*
OB0001: OFFSETS BETWEEN MEDIAN IMAGES

Image (1)	ΔRA (arcsec) (2)	ΔDEC (arcsec) (3)
1	0.0	0.0
2	3.7	10.0
3	10.0	13.0
4	19.8	9.1
5	22.4	2.1
6	18.2	−7.9
7	11.1	−10.8
8	0.7	−6.7
9	−2.8	0.4
10	−8.0	2.4
11	−3.4	4.4

NOTES: Col(1): Number of image. Col(2): Right Ascension offsets regarding of image 1 in arcsec. Col(3): Declination offsets regarding of image 1 in arcsec.

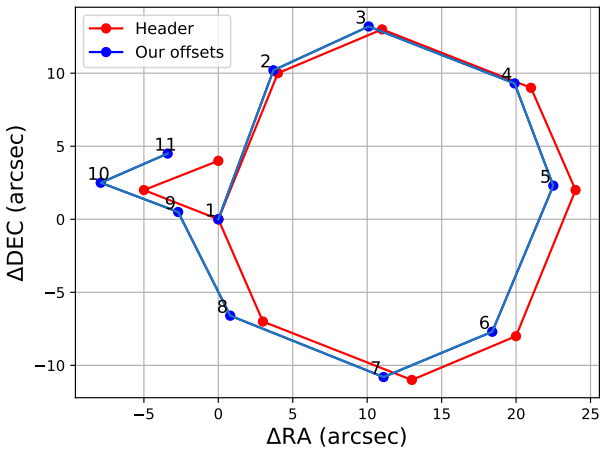

Figure 3.1: Dithering pattern of OB0001. Coordinates obtained from the header's information are shown in red, and coordinates measured with the bright star by us are shown in blue (error bars are too small).

3.3.2 OB0002, OB0003, OB0004 and OB0010

In the same way, the dithering patterns of OB0002 and OB0003 are shown in Figure 3.2 and dithering patterns of OB0004 and OB0010 in Figure 3.3.

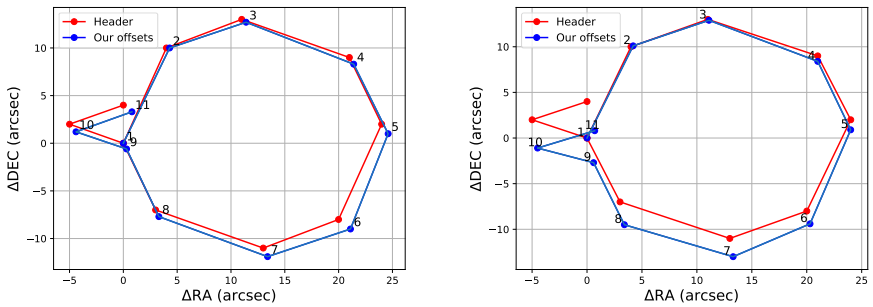

Figure 3.2: Dithering pattern of OB0002 (Left) and OB0003 (Right). Coordinates obtained from the header's information are shown in red, and coordinates measured with the bright star by us are shown in blue (error bars are too small).

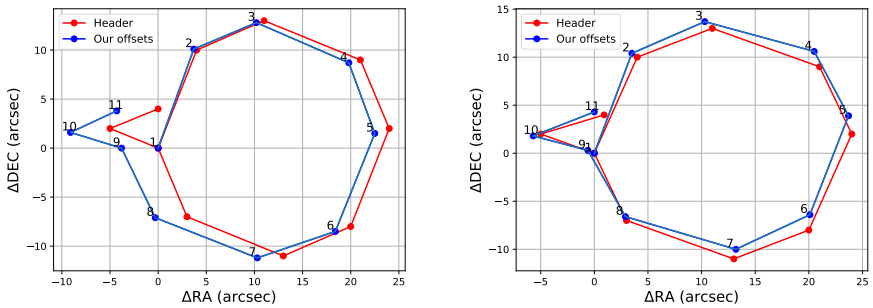

Figure 3.3: Dithering pattern of OB0004 (Left) and OB0010 (Right). Coordinates obtained from the header's information are shown in red, and coordinates measured with the bright star by us are shown in blue (error bars are too small).

3.3.3 Other OBs

Although there has not been time to reduce all the observing blocks, we have measured the offsets with both bright and faint reference stars, and we have refined these offsets by cross-correlation technique for the first 10 observing blocks, that is to say, we have the dithering patterns for 10 OBs. Since, as we have already mentioned, the offsets determined with the faint stars are not as reliable as the ones obtained with the bright one, we have used the latter to compare the dithering patterns of those 10 OBs (which are shown in Figure 3.4).

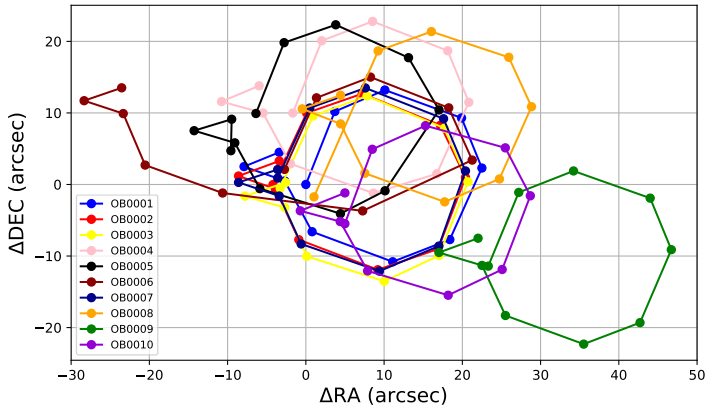

Figure 3.4: Dithering patterns of the first 10 observing blocks obtained by the cross-correlation technique using the bright reference star.

The study of this figure it is really interesting. According to the information of the headers, all the observing blocks (except OB0009) are taken in the same place and all have the same dithering pattern (except OB0006 and OB0008) (See Figure 2.1), but in fact there are offsets between all observing blocks. The displacement of OB0009 is specially remarkable (ΔDEC = -11.41 arcsec and ΔRA = -23.31 arcsec).

3.4 Final image

Finally, after months of hard work carrying out data reduction and combining final images of OB0001, OB0002, OB0003, OB0004 and OB0010, we have obtained the deep image (displayed in Figure 3.5 Right). We achieve to improve the ratio S/N and to be able to see some fainter objects. We have an image with a total exposure time around 16500s. Although the final image exhibits cosmetic defects, specially at the borders, an important fraction of the image area is useful for our scientific purposes. We identified the objects comparing our final image with the HST/WFC3 image of AEGIS-16 (Figure 3.5 Left).

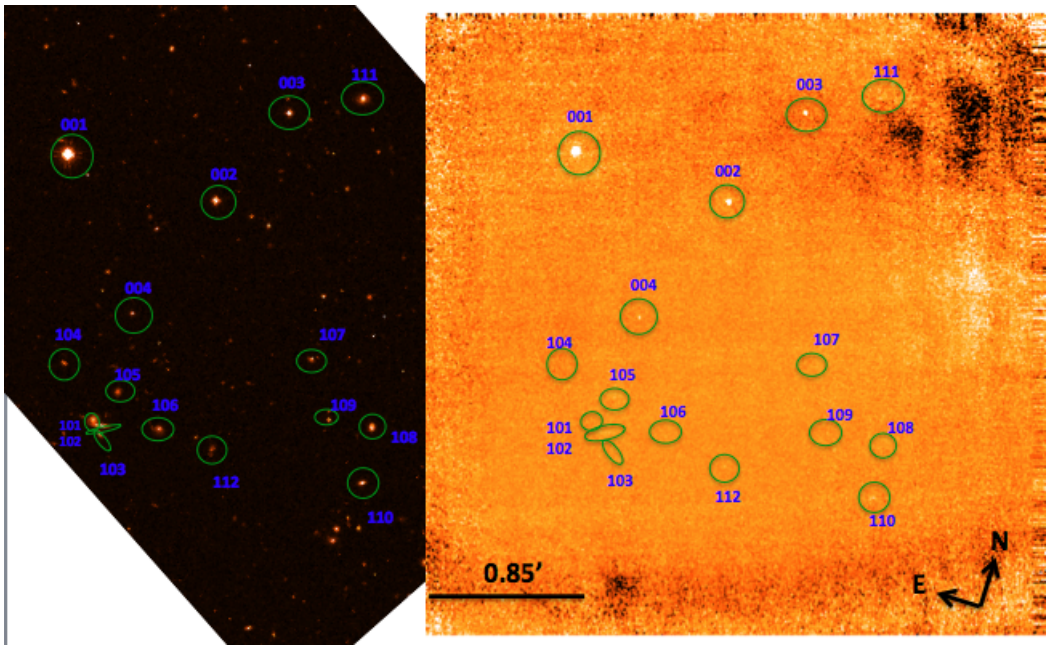

Figure 3.5: Region of observation. We identify 16 objects in the HST/WFC3 image (F125W filter, exposure time of 81028.46 s) of AEGIS-16 (Left), and in the same way, in our CIRCE deep image (ALBA NB filter, exposure time of 16500s) (Right)

A total of 16 objects have been identified. We looked for the objects in several catalogues such as NED (Ref: [13]), VizieR (Ref: [16]), Guide Star Catalog (Ref: [17]), Rainbow Cosmological Surveys database (Ref: [15]) and specially 3D-HST (Ref: [14]) in order to obtain more information about the candidates. We have elaborated two tables (differentiating between stars or galaxies) with the main parameters obtained from 3D-HST catalog about our found objects (See Tables 3.5 and 3.6). Ancillary information about each object can be found in *section 3.5 List of candidates*.
With 4.6 hours of exposure time with CIRCE in GTC we have obtained a limit magnitude of $\sim$ 22.31 (F125W filter). Note that usually Balmer 4000Åbreak and Lyman break can be used to derive redshifts for galaxies without emission lines. However, some galaxies have not these features, so it is not a reliable measure.

TABLE *3.5:*
PHYSICAL PROPERTIES ABOUT OBJECTS TYPE STAR: 3D-HST CATALOG AND CIRCE IMAGE

Object (1)	**id** (2)	**RA** (3)	**DEC** (4)	**class_STAR** (5)	**mag_F125W** (6)	**mag_NB** (7)	**SNR (NB)** (8)
001	17987	14:19:50.14	+52:54:03.74	1.00	14.82 ± 0.01	14.8 ± 0.1	19
002	22987	14:19:44.88	+52:53:47.89	0.90	17.32 ± 0.01	17.5 ± 0.2	6
003	26665	14:19:42.19	+52:54:15.76	0.85	17.97 ± 0.01	18.5 ± 0.3	3
004	17426	14:19:47.94	+52:53:11.91	0.87	19.53 ± 0.01	19.9 ± 0.5	2

NOTES: all the information has been obtained from AEGIS 3D-HST data release v4.1 (Ref: [14]). Col(1): Number of object. Col(2): Unique identifier number within AEGIS field. Col(3): Right Ascesion (hh:mm:ss). Col(4): Declination (dd:mm:ss). Col(5): Sextractor stellarity-index CLASS_STAR measured on the F160W image (and F140W where there is no coverage). Col (6): Total magnitude for F125W filter (ZP = 25). Col(7): Total magnitude for ALBA Narrow Band filter (ZP = 16.1). Col(8): signal-noise ratio in the ALBA Narrow Band filter.

TABLE *3.6:*
PHYSICAL PROPERTIES ABOUT OBJECTS TYPE GALAXY: 3D-HST CATALOGUE AND CIRCE IMAGE

Object (1)	**id** (2)	**RA** (3)	**DEC** (4)	$\mathbf{z_{spec}}$ (5)	$\mathbf{z_{peak}}$ (6)	**mag_F125W** (7)	**mag_NB** (8)	**SNR (NB)** (9)	**mag_u** (10)	**Size (kpc)** (11)
101	14438	14:19:49.40	+52:52:37.72	−1.00	0.29	19.59 ± 0.01	21.0 ± 1.3	1	21.88	2.19 × 2.09
102	14884	14:19:49.14	+52:52:35.82	0.51	0.69	19.29 ± 0.01	19.1 ± 0.5	2	22.40	6.63 × 1.63
103	14087	14:19:49.19	+52:52:33.10	0.45	0.39	19.59 ± 0.01	20.1 ± 0.8	1	22.24	2.49 × 1.57
104	14286	14:19:50.42	+52:52:56.22	0.68	0.62	21.25 ± 0.01	21.1 ± 2.7	1	23.28	2.76 × 1.62
105	15768	14:19:48.52	+52:52:46.59	0.05	0.06	20.66 ± 0.01	19.9 ± 0.7	2	21.98	0.46 × 0.40
106	16065	14:19:47.07	+52:52:34.38	−1.00	0.34	20.26 ± 0.01	20.4 ± 1.0	1	21.94	3.03 × 2.68
107	21027	14:19:41.57	+52:52:55.93	1.01	1.25	21.17 ± 0.01	20.1 ± 0.9	1	23.12	3.37 × 2.58
108	21350	14:19:39.46	+52:52:33.58	0.73	0.71	19.92 ± 0.01	21.0 ± 1.9	1	21.87	3.39 × 2.84
109	20243	14:19:40.99	+52:52:36.25	0.72	0.67	20.94 ± 0.01	20.5 ± 1.1	1	23.46	2.24 × 1.93
110	19786	14:19:39.84	+52:52:15.72	0.46	0.44	19.63 ± 0.01	20.1 ± 1.0	1	22.63	2.21 × 1.42
111	29415	14:19:39.54	+52:54:19.89	0.34	0.30	19.00 ± 0.01	20.1 ± 1.4	1	21.62	2.89 × 2.29
112	16025	14:19:45.14	+52:52:27.60	−1.00	1.53	22.31 ± 0.01	21.0 ± 1.3	1	23.48	2.02 × 1.33

NOTES: all the information has been obtained from AEGIS 3D-HST data release v4.1 (Ref: [14]). Col(1): Number of object. Col(2): Unique identifier number within AEGIS field. Col(3): Right Ascesion (hh:mm:ss). Col(4): Declination (dd:mm:ss). Col(5): Spectroscopic redshift (-1 if it not exists). Col(6): Photometric redshift at peak probability distribution. Col (7): Total magnitude for F125W filter (ZP = 25) and 1 sigma error. Col(8): Total magnitude for ALBA Narrow Band filter (ZP = 16.1). Col(9): signal-noise ratio in the ALBA Narrow-Band filter. Col (10): Total magnitude for filter SDSS/u (ZP = 25). Col(11): Size of the galaxy (semi-major axis × semi-minor axis) in kpc.

TABLE *3.7:*
DERIVED PROPERTIES OF OBJECTS TYPE GALAXY: 3D-HST CATALOGUE

Object (1)	**id** (2)	**Mass** ($\mathbf{M_\odot}$) (3)	**SFR** ($(\mathbf{M_\odot}/yr)$) (4)	**Av** (5)
101	14438	1.35×10^{10}	2.8	0.9
102	14884	1.62×10^{11}	24.6	2.0
103	14087	2.34×10^{10}	0.1	0.7
104	14286	8.51×10^{9}	1.4	1.9
105	15768	4.37×10^{7}	0.0	0.1
106	16065	6.31×10^{9}	1.7	0.4
107	21027	1.26×10^{11}	21.9	1.4
108	21350	7.41×10^{10}	39.8	1.4
109	20243	3.02×10^{10}	0.1	0.5
110	19786	4.27×10^{10}	0.1	0.5
111	29415	2.63×10^{10}	6.0	1.3
112	16025	4.79×10^{10}	0.3	2.1

NOTES: all the information has been obtained from AEGIS 3D-HST data release v4.1 (Ref: [14]). Col(1): Number of object. Col(2): Unique identifier number within AEGIS field. Col (3): Mass of the galaxy in solar masses. Col(4): Star Formation Rate in solar masses per year. Col(5): Dust attenuation in the V-band.

3.5 List of candidates

3.5.1 Object 001: id 17987. Type: star

This object has been identified in our final combined image and in the HST/WFC3 image (F125W filter). It is also the brightest star in our Field of view, and it has allowed us to measure the real offsets between images inasmuch as it has a total magnitude for F125W filter of 14.82. This star is found at RA: 14h 19m 50.14s and DEC: 52° 54' 03.74" (See object 001 in Table 3.5). Observing the Figure 3.6, object 001, we can see it has a blue color.

3.5.2 Object 002: id 22987. Type: star

This object has been identified in our final combined image and in the HST/WFC3 image (F125W filter). This star is found at RA: 14h 19m 44.88s and DEC: 52° 53' 47.89". It has a total magnitude for F125W filter of 17.32 (See object 002 in Table 3.5). Of our list of candidates, is the second brightest object, and in data reduction we were also able to measure the offsets with this star (previously called faint star). It helped us to check our offsets and to measure them when the main star of reference (object 001) appeared in the inactive channel of the detector. Observing the Figure 3.6 object 002, we can see it has a red color.

3.5.3 Object 003: id 26665. Type: star

This object has been identified in our final combined image and in the HST/WFC3 image (F125W filter). This star is found at RA: 14h 19m 42.19s and DEC: 52° 54' 15.76". It has a total magnitude for F125W filter of 17.97 (See object 003 in Table 3.5). This object was only observed in the final combined image (not in any step of data reduction). Observing the Figure 3.6, object 003, we can see it has a red color.

3.5.4 Object 004: id 17426. Type: star

This object has been identified in our final combined image and in the HST/WFC3 image (F125W filter). This star is found at RA: 14h 19m 47.94s and DEC: 52° 53' 11.91". It has a total magnitude for F125W filter of 19.53 (See object 004 in Table 3.5). This object is clearly observed in the final combined image (but not in any step of data reduction). It is the faintest star of our list of candidates (See Figure 3.6, object 004) .

3.5.5 Object 101: id 14438. Type: galaxy

This object has been identified in our final combined image and in the HST/WFC3 image (F125W filter). This galaxy is found at RA: 14h 19m 49.40s and DEC: 52° 52' 37.72". It has a total magnitude for F125W filter of 19.59 and a photometric redshift of z = 0.29 (spectroscopic redshift is not available), but perhaps the photometric redshift is wrong. The total magnitude for filter u (SDSS) is 21.88. The size of this galaxy is 2.19 kpc × 2.09 kpc (See object 101 in Table 3.6). This object was only observed in the final combined image (not in any step of data reduction), and it is a face-on barred spiral galaxy with some visible arms in color blue (due to star formation) and a bright core (See Figure 3.7, object 101). The galaxy has further a total mass about $1.35 \times 10^{10} M_{\odot}$ and a SFR $\sim 2.8\ M_{\odot}/yr$. The dust attenuation in V-band is 0.9 (See object 101 in Table 3.7).

3.5.6 Object 102: id 14884. Type: galaxy

This object has been identified in our final combined image and in the HST/WFC3 image (F125W filter). This galaxy is found at RA: 14h 19m 49.14s and DEC: 52° 52' 35.82". It has a total magnitude for F125W filter of 19.29 and a spectroscopic redshift of z = 0.51 (although it seems that this galaxy is in interaction with the previous galaxy (object 101), actually this galaxy is found behind the first, further away). The total magnitude for filter u (SDSS) is 22.40. The size of this galaxy is 6.63 kpc × 1.63 kpc (See object 102 in Table 3.6). This object was only observed in the final combined image (not in any step of data reduction), and is a edge-on disk galaxy (See Figure 3.7, object 102). The galaxy is really massive, with a total mass about $1.62 \times 10^{11} M_{\odot}$, and it has high SFR ($\sim 24.6\ M_{\odot}/yr$). The dust attenuation in V-band is 2.0 (See object 102 in Table 3.7).

3.5.7 Object 103: id 14087. Type: galaxy

This object has been identified in our final combined image and in the HST/WFC3 image (F125W filter). This galaxy is found at RA: 14h 19m 49.19s and DEC: 52° 52' 33.10". It has a total magnitude for F125W filter of 19.59 and a spectroscopic redshift of z = 0.45. The total magnitude for filter u (SDSS) is 22.24. The size of this galaxy is 2.49 kpc × 1.57 kpc (See object 103 in Table 3.6). This object was only observed in the final combined image (not in any step of data reduction), and is a edge-on galaxy where we can see clearly the bulge (See Figure 3.7, object 103). It is possible that it is a elliptical or lenticular galaxy with low star formation. The galaxy has a total mass about $2.34 \times 10^{10} M_{\odot}$ and a SFR $\sim 0.09\ M_{\odot}/yr$. The dust attenuation in V-band is 0.7 (See object 103 in Table 3.7).

3.5.8 Object 104: id 14286. Type: galaxy

This object has been identified in our final combined image and in the HST/WFC3 image (F125W filter). This galaxy is found at RA: 14h 19m 50.42s and DEC: 52° 52' 56.22". It has a total magnitude for F125W filter of 21.25 and a spectroscopic redshift of z = 0.68. The total magnitude for filter u (SDSS) is 23.28. The size of this galaxy is 2.76 kpc × 1.62 kpc (See object 104 in Table 3.6). This object was only observed in the final combined image (not in any step of data reduction). It is difficult to classify this galaxy (See Figure 3.7, object 104), may be it is a early type galaxy. The galaxy has further a total mass about $8.51 \times 10^{9} M_{\odot}$ and a SFR $\sim 1.4\ M_{\odot}/yr$. The dust attenuation in V-band is 1.9 (See object 104 in Table 3.7).

3.5.9 Object 105: id 15768. Type: galaxy

This object has been identified in our final combined image and in the HST/WFC3 image (F125W filter). This galaxy is found at RA: 14h 19m 48.52s and DEC: 52° 52' 46.59". It has a total magnitude for F125W filter of 20.66 and a spectroscopic redshift of z = 0.05. The total magnitude for filter u (SDSS) is 21.98. The size of this galaxy is 0.46 kpc × 0.40 kpc (See object 105 in Table 3.6). This object was only observed in the final combined image (not in any step of data reduction). It is a nearby dwarf irregular galaxy (See Figure 3.7, object 105). The galaxy has further a really low SFR $\sim 0.03\ M_{\odot}/yr$, and it is not a very massive galaxy, with a total mass about $4.37 \times 10^{7} M_{\odot}$. The dust attenuation in V-band is 0.1 (See object 105 in Table 3.7). It is one of the most interesting objects recovered so far and it is an excellent candidate to low mass Star-forming galaxy.

3.5.10 Object 106: id 16065. Type: galaxy

This object has been identified in our final combined image and in the HST/WFC3 image (F125W filter). This galaxy is found at RA: 14h 19m 47.07s and DEC: 52° 52' 34.38". It has a total magnitude for F125W filter of 20.26 and a photometric redshift of z = 0.34 (spectroscopic redshift is not available), but photometric redshift is not a reliable measure, often it is wrong. The total magnitude for filter u (SDSS) is 21.94. The size of this galaxy is 3.03 kpc × 2.68 kpc (See object 106 in Table 3.6). This object was only observed in the final combined image (not in any step of data reduction), and it seems a spiral galaxy interacting with other galaxy (See Figure 3.7, object 106). The galaxy has a total mass about $6.31 \times 10^{9} M_{\odot}$ and a SFR $\sim$ $1.7\ M_{\odot}/yr$. The dust attenuation in V-band is 0.4 (See object 106 in Table 3.7).

3.5.11 Object 107: id 21027. Type: galaxy

This object has been identified in our final combined image and in the HST/WFC3 image (F125W filter). This galaxy is found at RA: 14h 19m 41.57s and DEC: 52° 52' 55.93". It has a total magnitude for F125W filter of 21.17 and a spectroscopic redshift of z = 1.01 (becoming the most distant object of our list of candidates given z_{spec}). The total magnitude for filter u (SDSS) is 23.12. The size of this galaxy is 3.37 kpc × 2.58 kpc (See object 107 in Table 3.6). This object was only observed in the final combined image (not in any step of data reduction). It is an irregular galaxy (See Figure 3.7, object 107) . The galaxy has further a total mass about $1.26 \times 10^{11} M_{\odot}$ and a SFR $\sim 21.9\ M_{\odot}/yr$. The dust attenuation in V-band is 1.4 (See object 107 in Table 3.7).

3.5.12 Object 108: id 21350. Type: galaxy

This object has been identified in our final combined image and in the HST/WFC3 image (F125W filter). This galaxy is found at RA: 14h 19m 39.46s and DEC: 52° 52' 33.58". It has a total magnitude for F125W filter of 19.92 and a spectroscopic redshift of z = 0.73. The total magnitude for filter u (SDSS) is 21.87. The size of this galaxy is 3.39 kpc × 2.84 kpc (See object 108 in Table 3.6). This object was only observed in the final combined image (not in any step of data reduction). It is a face-on spiral galaxy with several tightly wrapped arms and a bright core (See Figure 3.7, object 108). The galaxy has a total mass about $7.41 \times 10^{10} M_{\odot}$ and a high SFR $\sim 39.8\ M_{\odot}/yr$. The dust attenuation in V-band is 1.4 (See object 108 in Table 3.7).

3.5.13 Object 109: id 20243. Type: galaxy

This object has been identified in our final combined image and in the HST/WFC3 image (F125W filter). This galaxy is found at RA: 14h 19m 40.99s and DEC: 52° 52' 36.25". It has a total magnitude for F125W filter of 20.94 and a spectroscopic redshift of z = 0.72. The total magnitude for filter u (SDSS) is 23.46. The size of this galaxy is 2.24 kpc × 1.93 kpc . (See object 109 in Table 3.6). This object was only observed in the final combined image (not in any step of data reduction). It is a elliptical galaxy (See Figure 3.7, object 109). The galaxy has further a total mass about $3.02 \times 10^{10} M_{\odot}$ and low SFR $\sim 0.1\ M_{\odot}/yr$. The dust attenuation in V-band is 0.5 (See object 109 in Table 3.7).

3.5.14 Object 110: id 19786. Type: galaxy

This object has been identified in our final combined image and in the HST/WFC3 image (F125W filter). This galaxy is found at RA: 14h 19m 39.84s and DEC: 52° 52' 15.72". It has a total magnitude for F125W filter of 19.63 and a spectroscopic redshift of z = 0.46. The total magnitude for filter u (SDSS) is 22.63. The size of this galaxy is 2.21 kpc × 1.42 kpc (See object 110 in Table 3.6). This object was only observed in the final combined image (not in any step of data reduction). It seems a lenticular or elliptical galaxy (See Figure 3.7, object 110). The galaxy has a total mass about $4.27 \times 10^{10} M_{\odot}$ and a low SFR $\sim 0.1\ M_{\odot}/yr$. The dust attenuation in V-band is 0.5 (See object 110 in Table 3.7).

3.5.15 Object 111: id 29415. Type: galaxy

This object has been identified in our final combined image and in the HST/WFC3 image (F125W filter). This galaxy is found at RA: 14h 19m 39.54s and DEC: 52° 54' 19.89". It has a total magnitude for F125W filter of 19.00 and a spectroscopic redshift of z = 0.34. The total magnitude for filter u (SDSS) is 21.62. The size of this galaxy is 2.89 kpc × 1.29 kpc (See object 111 in Table 3.6). This object was only observed in the final combined image (not in any step of data reduction). It is a barred spiral galaxy with bright core and two arms (See Figure 3.7, object 111). Furthermore, the galaxy has a total mass about $2.63 \times 10^{10} M_{\odot}$ and a SFR $\sim 6.0\ M_{\odot}/yr$. The dust attenuation in V-band is 1.3 (See object 111 in Table 3.7).

3.5.16 Object 112: id 16025. Type: galaxy

This object has been identified in our final combined image and in the HST/WFC3 image (F125W filter). This galaxy is found at RA: 14h 19m 45.14s and DEC: 52° 52' 27.60". It has a total magnitude for F125W filter of 22.31 (becoming the faintest object of our list of candidates) and a photometric redshift of z = 1.53 (spectroscopic redshift is not available). If this photometric redshift is correct, this extend object would be the most distant object of our list of candidates. The total magnitude for filter u (SDSS) is 23.48. The size of this galaxy is 2.02 kpc × 1.33 kpc (See object 112 in Table 3.6). This object was only observed in the final combined image (not in any step of data reduction). It is an irregular galaxy (See Figure 3.7, object 112) . The galaxy has further a total mass about $4.79 \times 10^{10} M_{\odot}$ and a low SFR $\sim 0.3\ M_{\odot}/yr$. The dust attenuation in V-band is 2.1 (See object 112 in Table 3.7).

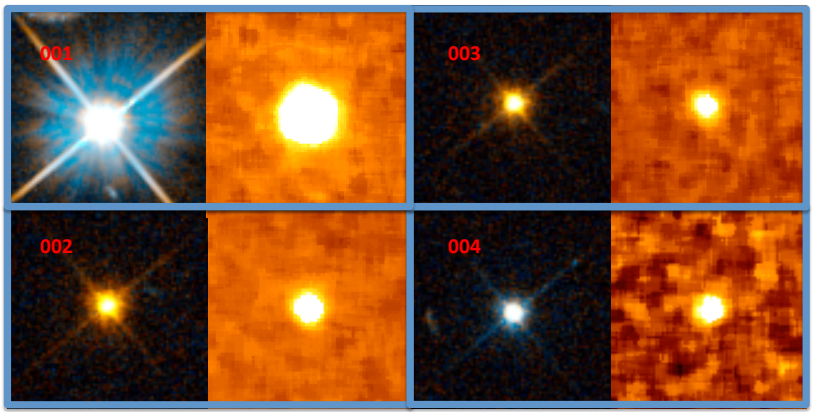

Figure 3.6: Identified objects type star (See Table 3.5). Left: object in color mosaic of HST (Filters: optical V band (555 nm) and pseudogreen V+I bands, Infrared I band (814 nm)). Right: object in CIRCE image (Filter: ALBA Narrow Band). The image was smoothed applying a median filter in order to observe better the objects. North is 218° right of the vertical. Box size: 8 arcsec × 8 arcsec

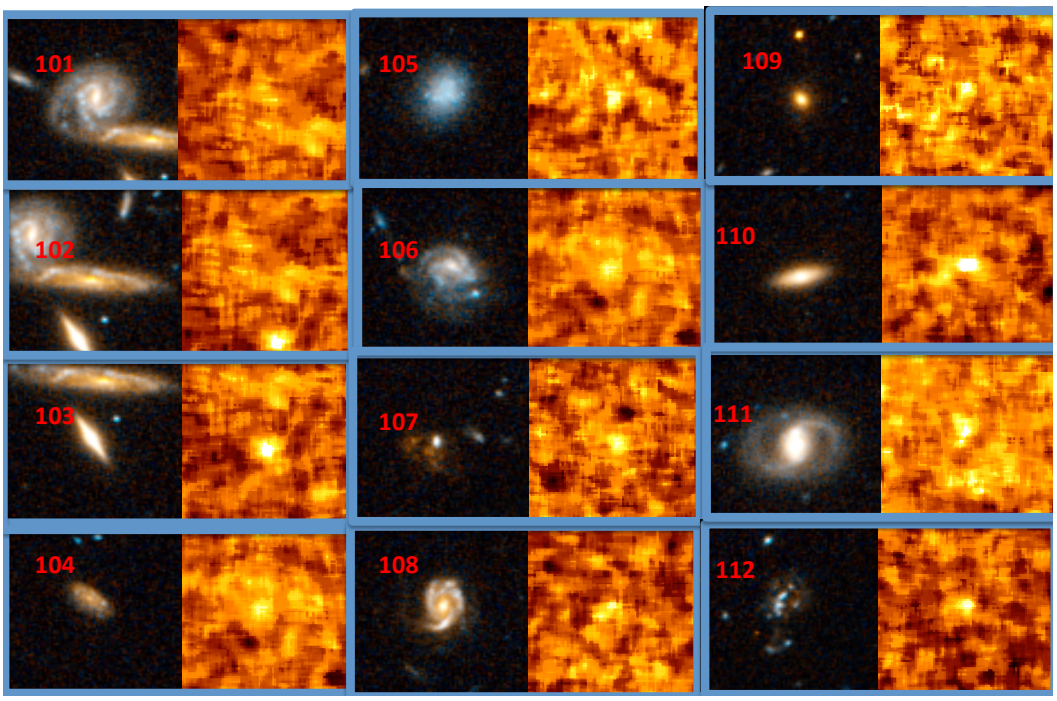

Figure 3.7: Identified objects type galaxy (See Table 3.6) . Left: object in color mosaic of HST (Filters: optical V band (555 nm) and pseudogreen V+I bands, Infrared I band (814 nm)). Right: object in CIRCE image (Filter: ALBA Narrow Band). The image was smoothed applying a median filter in order to observe better the objects. Orientation: North is 218° right of the vertical. Box size: 8 arcsec × 8 arcsec

3.6 Overall scientific analysis

Star Forming Galaxies (SFGs) show a strong correlation between their star formation rate (SFR) and stellar mass ($M_\star$), and this correlation may show slight variations with the redshift (the SFR steadily increases at fixed mass with increasing redshift). Our identified galaxies are in the bin $0.04 < z < 1.54$ and the log(SFR) - log($M_\star$) relation is shown in Figure 3.8 (Right), where stands out the object 105 of our list of candidates which is a low-mass nearby galaxy with low SFR. In addition to this, the most massive galaxies (objects 102, 107 and 108) are also those that present greater star formation coinciding with relatively high values of spectroscopic redshifts (z = 0.51, 1.01 and 0.73 respectively). These types of diagrams indicate that the galaxies were forming stars at much higher rates in the distant universe relative to today.

A color-color diagram is shown in Figure 3.8 (Left). In the plot we observe that the object 105 has also the most blue color of our list of candidates, followed by the object 106. The elliptical galaxies (objects 109 and 110) presents red colors as expected. The red colors may be attributed to dust, although older stellar populations have similarly red colors. The results are in good agreement with the observed colors in the color-mosaic of HST (Figure 3.7). The objects in the top left of the diagram correspond with quiescents galaxies, without young stellar population.

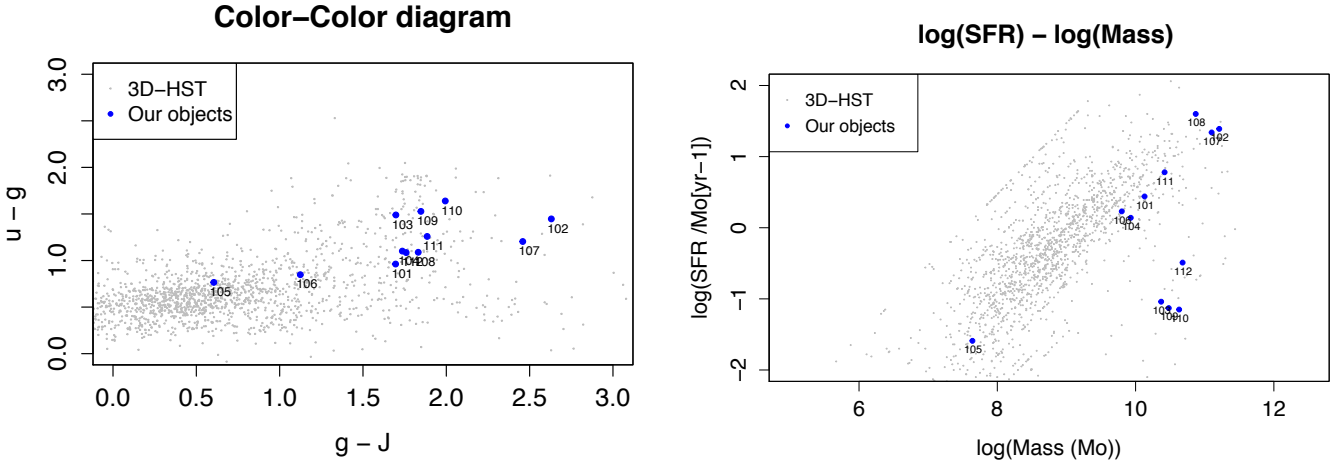

Figure 3.8: Left: Rest-frame ugJ diagram of the galaxies of AEGIS-16 3D-HST (gray) and our identified galaxies (blue). Right: log(SFR)-log(Mass) relation of the galaxies of AEGIS-16 3D-HST (gray) and our identified galaxies (blue). Data obtained from AEGIS 3D-HST data release v4.1. (Ref: [14])

In spite of we have identified only 12 galaxies, we have displayed the distribution of all the objects of AEGIS-16 field in Figure 3.9. We have photometric redshifts for 1923 objects, although a more reliable measure is the spectroscopic redshift but only the data for 53 objects are available. In the histogram of spectroscopic redshift we can see a peak around $z \sim 0.7$. The spectroscopic redshifts of our identified galaxies are marked with red color.

In a first attempt to select candidates of Lyman α emitters, a color-magnitude diagram of the 16 identified objects is shown in Figure 3.10 (the stars are marked in red and the galaxies in blue). We compared the magnitude in F125W filter with the magnitude in our Narrow Band filter in order to detect Lyman Alpha Emitters due to the flux excess in the Alba Narrow Band filter. It's still soon to select candidates because our list of objects is not very extensive yet. In this type of diagram the dispersion may be originated due to the intrinsic color of each object, although in our case because of the current quality of our deep image, objects with magnitude in F125W filter > 19 show significant dispersion. Moreover, it exists the possibility that different sensibilities in the two filter yield asymmetry in the diagram (the flux of our objects can be overestimated). We have performed an accurate measure of the flux in the NB filter for the stars, but the error bars for the galaxies are quite significant. The color-magnitude diagram will change as the number of identified objects increases and the quality improves.

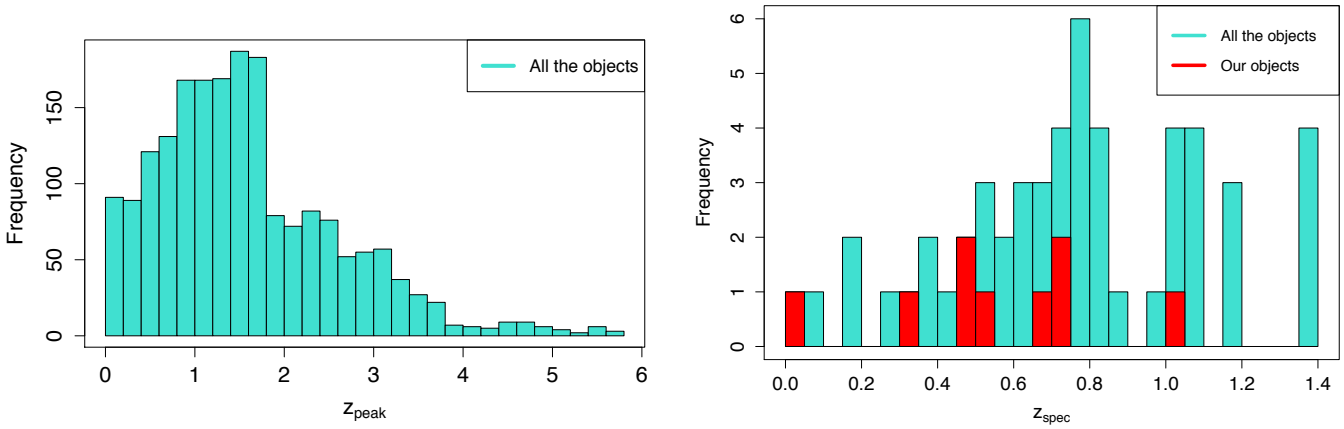

Figure 3.9: Histogram of the distribution of all the objects of AEGIS-16 field as from photometric redshift (Left) and spectroscopic redshift (Right) according to AEGIS 3D-HST data release v4.1. (Ref: [14]) where the redshift of our objects are marked in red. Note that photometric redshift is available for 1923 objects but spectroscopic redshift only for 53 objects.

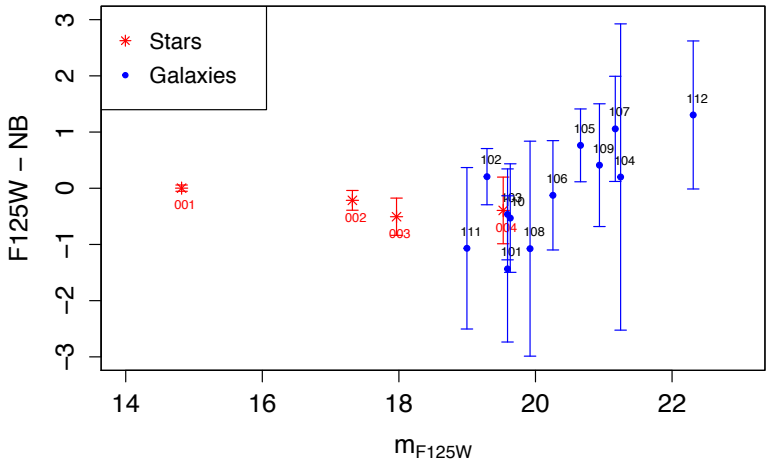

Figure 3.10: Color-magnitude diagram of the 16 identified objects (stars in red and galaxies in blue). Magnitudes in F125W have been obtained from AEGIS 3D-HST data release v4.1. (Ref: [14]), and magnitudes in the Narrow Band filter have been obtained from the photometric calibration of the final deep image of 16500s of exposure time (Figure 3.5 Right) taken with CIRCE.

With our deep image of 16500s of exposure time we have achieved a limit magnitude of 22.3 in F125W (object 112). Our expectations are to obtain an image with four times more exposure time, and thus we want to increase the limit magnitude a value of ~ 1.6. Therefore, with 23 observing blocks we estimate that the limit magnitude will be around m ~ 24. If the Lyman α emitters are so bright like the luminous galaxy found by Zitrin et al. 2015 (Ref: [12]), we can be able to detect them.

Chapter 4

Conclusions

Working with infrared data is quite complicated when it comes to data reduction. The large amount of data at our disposal requires the existence of codes to handle this data easily and process the information in the shortest time possible. Despite of the data reduction techniques employed, the final image still shows invalid regions due to the poor cosmetic of the detector. The borders are not fully useful.
Observing the dithering patterns it makes us think it is possible that the telescope provides an accumulated error in the tracking but we are not sure at all. It should be noted that initially we started working with the first ten observing blocks, but after the discovery of offsets between ramps it was necessary to modify programming codes, elaborate new codes, and think new strategies to solve the problems that were emerging. Solving the problem of offsets between ramps has taken us weeks of work. Performing 5 ramps is better than 3 ramps since it has allowed us to correct the bad tracking of the GTC and do not get elongated stars. Interpolating defective pixels slowed down the project but we improved the technique and we obtained better results. Thereby we have only five observing blocks totally reduced (OB0001, OB0002, OB0003, OB0004 and OB0010). Currently we have an image with exposure time around 16500s with a nIR camera in GTC but we have more observing blocks to reduce and to add, so the signal-to-noise ratio and the quality of the deep image will improve. We have not achieved the depth that we expected. The detection limit of our study is a magnitude 22.31 in F125W filter (the faintest object identified). Finally, we present a list of 16 candidates (4 stars and 12 galaxies) identified in both our CIRCE image (ALBA Narrow Band filter) and HST/WFC3 image (F125W filter). 3D-HST survey has allowed us to obtain ancillary information about these objects. We have performed a scientific analysis of some properties of our identified galaxies and all the results are in good agreement with the expectations. However, we need a more extensive sample to carry out a more detailed scientific analysis. For the time being, no unidentified object already.

The study of high redshift galaxies is key to understand the process of reionization of the Universe and elaborate models of formation and evolution of the galaxies. In this observational test we can not confirm or reject the double reionization scenario predicted by AMIGA model (Salvador-Solé 2015). We need to reduce more observing blocks in order to reach more depth in the final image.

Chapter 5

Future work

This is still a work in progress, and new results will come in the next few months. After the study, we expect to publish the most important results of this effort. For the moment, our next steps are to improve the methods inside *imcombine* program to try to remove better the effect of cosmetic defects of the detector, and thus obtain a deep image with better quality. Moreover, we have to finish to reduce all the observing blocks (nowadays we have 23 already observed, only 5 of them are totally reduced). If we don't find new problems, we hope to progress faster with the data reduction. It must be borne in mind that we are looking for really faint objects, and although we have the opportunity to use the GTC, a lot of exposure time is necessary to achieve the detection limit. With 23h of exposure time we expect to be able to reach a magnitude of ~ 24 in our Narrow Band filter.

Finally, we will elaborate a list of candidates with Lyman alpha emission. By comparing the flux excess in the ALBA narrow-band filter with the broad band filter J, we can select some of them as possible Lyman Alpha Emitters at z $\sim$ 9.3. However the contaminants owing other emission lines at others redshifts have to be eliminated. For this reason, spectroscopy is necessary. If we find any LAE at this z, we could confirm the double reionization scenario predicted by AMIGA model (Salvador-Solé 2015), and these early objects (faint and low mass galaxies) would be the building blocks of present-day galaxies and the main source of the ionizing photons responsible for reionization.

Many advances have been made in the last years on the study of the high z Universe and the size of galaxy surveys has been increased but many questions remain and the uncertainty on ther Epoch of Reionization is large. Not only is the timing of reionization poorly constrained, but the mechanism that causes it is equally uncertain. There are other research groups seeking the most distant objects and working in this topic. Future facilities such as the James Webb Space Telescope, the 30-m-class ground-based telescopes or a new generation of sensitive, multi-object near-infrared spectrographs will provide a much more detailed view of the early Universe.

References

[1] B.Clément, J-G. Cuby, F.Courbin et al. , 2012, A&A, 538, A66. *"Evolution of the observed Lyα luminosity function from z = 6.5 to z = 7.7: evidence for the epoch of reionization?"*

[2] M. Dijkstra, J.S.B. Wyithe and Z. Haiman, 2007, MNRAS, 379, 253–259, *"Luminosity functions of Ly emitting galaxies and cosmic reionization of hydrogen"*

[3] C.Gómez-Guijarro, J.Gallego, V. Villar et al. , 2016, A&A, 591,151 , *"Properties of galaxies at the faint end of the Hα luminosity function at z ∼ 0.62"*

[4] A. Manrique, E. Salvador-Solé, E. Juan et al. , 2015, ApJ, 216:13, *"Leaving the Dark Ages with AMIGA"*

[5] P.A. Oesch, G.Brammer, P.G. van Dokkum et al. , 2016, ApJ, Volume 819, 129, *"A remarkably luminous galaxy at z=11.1 measured with Hubble Space Telescope Grism Spectroscopy"*

[6] B.E. Robertson, R.S. Ellis, J.S. Dunlop et al. , 2010, Nature, 468, *"Early star-forming galaxies and the reionization of the Universe"*

[7] B.E. Robertson, S.R. Furlanetto, E. Schneider et al. , 2013, ApJ, 768:71, *"New constraints on cosmic reionization from the 2012 Hubble Ultra Deep Field Campaign"*

[8] E. Salvador-Solé, 2015, *"Constraints on Reionization from the Observed Properties of the High-z Universe."*

[9] J. Taylor and A. Lidz, 2013, MNRAS, 437, 2542–2553, *"What do observations of the Lyman fraction tell us about reionization?"*

[10] V. Villar, J. Gallego, P.G.Pérez et al. , 2008, ApJ, 677, 169-185, *"The Hα-based star formation rate density of the Universe at z= 0.84"*

[11] E. Zackrisson, C. Binggeli, K. Finlator et al. , 2016, ApJ, Volume 836, *"The spectral evolution of the First Galaxies. III. Simulated James Webb Space Telescope spectra of reionization-epoch galaxies with Lyman continuum leakage"*

[12] A. Zitrin, I.Labbé, S. Belli et al. , 2015, ApJ, 810 , L12, *"Lyα emission from a luminous z= 8.68 galaxy : Implications for galaxies as tracers of cosmic reionization"*

[13] NASA Extragalactic Database: http://ned.ipac.caltech.edu/

[14] 3D-HST research: http://3dhst.research.yale.edu/

[15] Rainbow Cosmological Surveys database: http://rainbowx.fis.ucm.es/

[16] VizieR database: http://vizier.u-strasbg.fr/viz-bin/VizieR

[17] MAST Guide Star Catalogs: https://archive.stsci.edu/gsc/

[18] GTC website: http://www.gtc.iac.es/instruments/circe/

[19] CIRCE website: http://www.astro.ufl.edu/CIRCE/

[20] Observation proposal for the GTC provided by Jesús Gallego Maestro.

[21] http://reduceme.readthedocs.io/en/latest/

Chapter 6

Appendix

6.1 Programming code

Below the code for the section of data reduction developed in Python:

- ***reduce.py***

This script establishes the first part of the reduction. We use this script to read the raw images and generate coadded result and the individual ramps. Moreover we obtain the averaged dark (as from list of darks)

```
from __future__ import division
from __future__ import print_function
import argparse
from astropy.io import fits
import numpy as np



def read_raw_circe(infile, nramps, outfile, debug=0):
    """Read raw CIRCE ramp and generate coadded result.

    Parameters
    ----------
    infile : string
        Input file name containing the individual reads along the
        different ramps.
    nramps : int
        Number of ramps.
    outfile : string
        Output file name corresponding to the result of coadding all
        the ramps.
    debug : int
        debug=0: no additional information is generated
        debug=1: save ramps
        debug=2: save ramps and individual reads in the ramps

    """

    print("\n* Working with image:\n" + infile)
    hdulist = fits.open(infile)
    main_header = hdulist[0].header
    # remove header keywords that are not FITS standard
    for wrong_keywords in ['CD1_1', 'CD1_2', 'CD2_1', 'CD2_2']:
        main_header.remove(wrong_keywords)
    # set keywords to be requested by imcombine
    main_header.set('TELESCOP', 'GTC', 'Telescope name (for imcombine)')
    airmass1 = main_header.get('AIRMASS1')
```

```
    airmass2 = main_header.get('AIRMASS2')
    airmass = (airmass1 + airmass2) / 2
    main_header.set('AIRMASS', airmass,
                    'Airmass (average of AIRMASS1 and AIRMASS2)',
                    before='AIRMASS1')
    lista_rampas = []
    for i in range(nramps):
        print("   - reading ramp " + str(i+1))
        image2d_1 = hdulist[2*i+1].data.astype(np.float)
        image2d_2 = hdulist[2*i+2].data.astype(np.float)
        if debug==2:
            hdu = fits.PrimaryHDU(image2d_1)
            dumfile = infile[:-5] + "_ext" + str(2*i+1) + ".fits"
            hdu.writeto(dumfile, clobber=True)
            hdu = fits.PrimaryHDU(image2d_2)
            dumfile = infile[:-5] + "_ext" + str(2*i+2) + ".fits"
            hdu.writeto(dumfile, clobber=True)
        result = image2d_2 - image2d_1
        if debug==1 or debug==2:
            hdu = fits.PrimaryHDU(result)
            dumfile = infile[:-5] + "_ramp" + str(i+1) + ".fits"
            hdu.writeto(dumfile, clobber=True)
        lista_rampas.append(result)
    hdulist.close()

    result = np.copy(lista_rampas[0])
    if nramps > 1:
        for i in range(1, nramps):
            result += lista_rampas[i]

    result /= nramps
    # save output file
    hdu = fits.PrimaryHDU(result, main_header)  # add main_header
    hdu.writeto(outfile, clobber=True)
    print("\nGenerating output file:\n" + outfile)

def average_frames(list_of_frames, outfile, iheader=0):
    """Compute averaged frame from list of frames.

    Parameters
    ----------
    list_of_frames : list of strings
        List containing the list of invidual FITS files to be avaraged.
    outfile : string
        Outpuf file name
    iheader : int
        Image number (in list_of_frames) from which the header will
        be copied. If 0, no header is added to the output file.

    """

    nframes = len(list_of_frames)

    main_header = None

    for i in range(nframes):
        infile = list_of_frames[i]
        print("\n*Working with file:\n", infile)
        hdulist = fits.open(infile)
        if i == iheader:
            main_header = hdulist[0].header
        image2d = hdulist[0].data.astype(np.float)
        hdulist.close()
        if i == 0:
            result = np.copy(image2d)
```

```
        else:
            result += image2d

    result /= nframes
    if main_header is None:
        hdu = fits.PrimaryHDU(result)
    else:
        hdu = fits.PrimaryHDU(result, main_header)  # add main_header
    hdu.writeto(outfile, clobber=True)
    print("\n*Generating output file:\n" + outfile)

if __name__ == "__main__":

    parser = argparse.ArgumentParser(prog='reduce')
    parser.add_argument("input_darks",
                        help="txt file with list of initial darks")
    parser.add_argument("input_objects",
                        help="txt file with list of initial images")

    parser.add_argument("nramps",
                        help="number of ramps",type=int)
    args = parser.parse_args()

    list_darks = np.genfromtxt(args.input_darks, dtype=[('darksname', '|S100')])
    darksname = list_darks['darksname']

    list_objects = np.genfromtxt(args.input_objects, dtype=[('objectsname', '|S100')
        ])
    objectsname = list_objects['objectsname']

    nramps = int(args.nramps)


    execute_darks = True
    # compute averaged dark
    if execute_darks:
        list_darks_coadd = []
        for infile in darksname:
            outfile = infile[:-5] + "_coadd.fits"
            list_darks_coadd.append(outfile)
            read_raw_circe(infile, nramps, outfile)
        average_frames(list_darks_coadd, "dark.fits", iheader=0)

    execute_objects = True

    if execute_objects:

        list_object_coadd = []
        for infile in objectsname:
            outfile = infile[:-5] + "_coadd.fits"
            list_object_coadd.append(outfile)
            read_raw_circe(infile, nramps, outfile, debug=1)
```

- ***mide_offsets.py***

This script calculates the offsets by cross-correlation technique as from a list with initial offsets. We use this script to obtain the offsets between ramps and the offsets between images in each observing block.

```
from __future__ import division
from __future__ import print_function
from astropy.io import fits
import argparse
import matplotlib.pyplot as plt
import numpy as np
import re
from skimage.feature import register_translation
from pause_debugplot import pause_debugplot


def readfits(infile, iext=0):
    """Read FITS file.

    Parameters
    ----------
    infile : string
        Input file name to be read.
    iext : int
        Extension number (0=first HDU)

    Returns
    -------
    image2d : 2d numpy array, floats
        Data array.
    main_header: fits header
        Primary header.
    header : fits header
        Header corresponding to the extension read. When the extension
        is zero, 'header' and 'main_header' are the same.

    """

    hdulist = fits.open(infile)
    main_header = hdulist[0].header
    header = hdulist[iext].header
    image2d = hdulist[iext].data.astype(np.float)
    hdulist.close()

    return image2d, main_header, header


def cross_correlate(ref_image, shifted_image, debugplot=0):
    """Cross-correlation to identify the relative shift.

    Parameters
    ----------
    ref_image : 2d numpy array (float)
        Reference image.
    shifted_image : 2d numpy array (float)
        Shifted image.
    debugplot : int
        Determines whether intermediate computations and/or plots
        are displayed:
        00 : no debug, no plots
        01 : no debug, plots without pauses
        02 : no debug, plots with pauses
        10 : debug, no plots
        11 : debug, plots without pauses
        12 : debug, plots with pauses
```

```
    Returns
    -------
    shifts : ndarray
        Shift vector (in pixels) required to register ``shifted_image``
         with ``reference``. Axis ordering is consistent with numpy
         (e.g. Z, Y, X).
    error : float
        Translation invariant normalized RMS error between
        ``reference`` and ``shifted_image``.
    phasediff : float
        Global phase difference between the two images (should be
        zero if images are non-negative).

    """

    shifts, error, diffphase = \
        register_translation(ref_image, shifted_image)

    if debugplot >= 10:
        print(">>> Offset (y, x):", shifts)
        print(">>> Error.....:", error)
        print(">>> Diffphase....:", diffphase)

    if debugplot % 10 != 0:
        fig = plt.figure(figsize=(12, 5))
        ax1 = plt.subplot(1, 3, 1, adjustable='box-forced')
        ax2 = plt.subplot(1, 3, 2, sharex=ax1, sharey=ax1,
                          adjustable='box-forced')
        ax3 = plt.subplot(1, 3, 3, sharex=ax1, sharey=ax1,
                          adjustable='box-forced')

        ax1.imshow(ref_image, interpolation='nearest', origin='low')
        # ax1.set_axis_off()
        ax1.set_title('Reference image')

        ax2.imshow(shifted_image, interpolation='nearest', origin='low')
        # ax2.set_axis_off()
        ax2.set_title('Offset image')

        # View the output of a cross-correlation to show what the
        # algorithm is doing behind the scenes
        image_product = np.fft.fft2(ref_image) * \
                        np.fft.fft2(shifted_image).conj()
        cc_image = np.fft.fftshift(np.fft.ifft2(image_product))
        ax3.imshow(cc_image.real, interpolation='nearest', origin='low')
        # ax3.set_axis_off()
        ax3.set_title("Cross-correlation")

        plt.show(block=False)
        plt.pause(0.001)
        pause_debugplot(debugplot)
        plt.close()

    return shifts, error, diffphase

if __name__ == "__main__":

    parser = argparse.ArgumentParser()
    parser.add_argument("input_list",
                        help="txt file with list of initial images")
    parser.add_argument("input_offsets",
                        help="txt file (from xnirspec) with list of" + \
                        "initial offsets")
    parser.add_argument("x0",
```

```
                    help="x0 coordinate corresponding to object in image")
parser.add_argument("y0",
                    help="y0 coordinate corresponding to object in image")
parser.add_argument("delta_x",
                    help="x-width of the image subregion to be employed")
parser.add_argument("delta_y",
                    help="y-width of the image subregion to be employed")
parser.add_argument("--dont_subtract_consecutive",
                    help="avoid subtraction of  consecutive images",
                    action="store_true")
parser.add_argument("--dark_name",
                    help="file name of the dark file (default: dark.fits)",
                    default="dark.fits")
parser.add_argument("--debugplot",
                    help="integer indicating plotting/debugging" + \
                    " (default=0)", type=int,
                    default=0)
args = parser.parse_args()

x0 = int(args.x0)
y0 = int(args.y0)
delta_x = int(args.delta_x)
delta_y = int(args.delta_y)

list_files = np.genfromtxt(
    args.input_list, dtype=[('filename', '|S100')])
list_offsets = np.genfromtxt(
    args.input_offsets,
    dtype=[('iflag', '<i8'), ('filename', '|S100'),
           ('offx', '<i8'), ('offy', '<i8')]
)
#filename = list_offsets['filename']
filename = list_files['filename']
offx = list_offsets['offx']
offy = list_offsets['offy']
nfiles = filename.size

for val in zip(filename, offx, offy):
    print(val)

list_regions = []
for k in range(nfiles):
    if k < nfiles - 1:
        image1, dum, dum = readfits(filename[k])
        image2, dum, dum = readfits(filename[k + 1])
    else:
        image1, dum, dum = readfits(filename[k])
        image2, dum, dum = readfits(filename[k - 1])

    if args.dont_subtract_consecutive:
        image = image1
    else:
        image = image1 - image2


    i1 = int(y0 - delta_y/2 - offy[k])
    i2 = int(y0 + delta_y/2 - offy[k])
    j1 = int(x0 - delta_x/2 - offx[k])
    j2 = int(x0 + delta_x/2 - offx[k])
    sublist_regions = []
    npixstep=3  # step size (in pixels)
    number_of_semisteps = 3  # at both sides of the initial position
    for deltai in np.arange(-number_of_semisteps, number_of_semisteps+1, 1,
        dtype=int)*npixstep:
        for deltaj in np.arange(-number_of_semisteps, number_of_semisteps+1, 1,
```

```
                dtype=int)*npixstep:
                region = image[(i1+deltai):(i2+deltai), (j1+deltaj):(j2+deltaj)]
                sublist_regions.append(region)
        list_regions.append(sublist_regions)

    sublist_reference = list_regions[0]
    for k in range(1,nfiles):
        sublist_offset_region = list_regions[k]
        if args.debugplot >= 10:
            print("* Reference image:", filename[0])
            print("* Offset image...:", filename[k])
        l = 0
        offx_tmp = np.zeros((2*number_of_semisteps+1)*(2*number_of_semisteps+1))
        offy_tmp = np.zeros((2*number_of_semisteps+1)*(2*number_of_semisteps+1))
        for deltai in np.arange(-number_of_semisteps, number_of_semisteps+1 ,1,
            dtype=int)*npixstep:
            for deltaj in np.arange(-number_of_semisteps, number_of_semisteps+1, 1,
                dtype=int)*npixstep:
                tmp_reference = sublist_reference[l]
                tmp_offset_region = sublist_offset_region[l]
                shifts, error, diffphase = \
                    cross_correlate(tmp_reference, tmp_offset_region, debugplot=args
                        .debugplot)
                offx_tmp[l] = shifts[1]
                offy_tmp[l] = shifts[0]
                print('>>>', l, shifts[0], shifts[1])
                l += 1
        print(offx_tmp)
        print(offy_tmp)
        print('>>> median offx, std offx: ', np.median(offx_tmp), np.std(offx_tmp))
        print('>>> median offy, std offy: ', np.median(offy_tmp), np.std(offy_tmp))
        offy[k] += np.median(offy_tmp)
        offx[k] += np.median(offx_tmp)
        print(k, offx[k], offy[k])


    print("--- ooo ---")
    for val in zip(filename, offx, offy):
        print(val)

    list_offsets['filename'] = list_files['filename']
    output_txt = re.sub('.txt\$', '_refined.txt', args.input_offsets)
    np.savetxt(output_txt, list_offsets,
               fmt="\%1d \%s " + args.dark_name + " \%6d \%6d")
```

- ***generate_consecutive_subtracted.py***

We use this script to subtract consecutive images, thus we achieve to remove noise and see better the objects to measure the offsets.

```
from __future__ import division
from __future__ import print_function
import argparse
from astropy.io import fits
import numpy as np
import re


def readfits(infile, iext=0):
    """Read FITS file.

    Parameters
    ----------
    infile : string
        Input file name to be read.
    iext : int
        Extension number (0=first HDU)

    Returns
    -------
    image2d : 2d numpy array, floats
        Data array.
    main_header: fits header
        Primary header.
    header : fits header
        Header corresponding to the extension read. When the extension
        is zero, 'header' and 'main_header' are the same.

    """

    hdulist = fits.open(infile)
    main_header = hdulist[0].header
    header = hdulist[iext].header
    image2d = hdulist[iext].data.astype(np.float)
    hdulist.close()

    return image2d, main_header, header


if __name__ == "__main__":

    # define expected command-line arguments
    parser = argparse.ArgumentParser()
    parser.add_argument("input_list",
                        help='"txt file with list of initial file names"')
    parser.add_argument("nramps",
                        help="number of ramps",type=int)
    args = parser.parse_args()

    nramps = int(args.nramps)

    # read list with file names
    list_files = np.genfromtxt(args.input_list, dtype=[('filename', '|S100')])
    filename = list_files['filename']

    nfiles = filename.size

    filename_cs = np.copy(filename)
```

```
# subtract consecutive images
for k in range(nfiles):
    if k < nfiles - nramps:
        print("image1: ", filename[k])
        print("image2: ", filename[k+nramps])
        image1, main_header, dum = readfits(filename[k])
        image2, dum, dum = readfits(filename[k + nramps])
    else:
        print("image1: ", filename[k])
        print("image2: ", filename[k-nramps])
        image1, main_header, dum = readfits(filename[k])
        image2, dum, dum = readfits(filename[k - nramps])
    image = image1 - image2

    outfile = re.sub('.fits\$', '_cs.fits', filename[k])
    print("Generating:" + outfile)
    hdu = fits.PrimaryHDU(image, main_header)
    hdu.writeto(outfile, clobber=True)
    filename_cs[k] = outfile

output_txt = re.sub('.txt\$', '_cs.txt', args.input_list)
np.savetxt(output_txt, filename_cs, fmt="\%s")
print("\nExporting list with new files to:", output_txt)
```

- ***median_of_ramps.py***

This script allow us to correct the offsets between ramps and to generate a datacube of these ramps. Finally, it computes the median of this datacube that we use like final image.

```
from __future__ import division
from __future__ import print_function
from astropy.io import fits
import argparse
import numpy as np
import re
import sys


def readfits(infile, iext=0):
    """Read FITS file.

    Parameters
    ----------
    infile : string
        Input file name to be read.
    iext : int
        Extension number (0=first HDU)

    Returns
    -------
    image2d : 2d numpy array, floats
        Data array.
    main_header: fits header
        Primary header.
    header : fits header
        Header corresponding to the extension read. When the extension
        is zero, 'header' and 'main_header' are the same.

    """

    hdulist = fits.open(infile)
    main_header = hdulist[0].header
    header = hdulist[iext].header
    image2d = hdulist[iext].data.astype(np.float)

    # Only to ckeck the images dimensions
    NAXIS1 = main_header.get('NAXIS1')
    NAXIS2 = main_header.get('NAXIS2')
    # print(NAXIS1)
    # print(NAXIS2)

    hdulist.close()

    return image2d, main_header, header


def trimming_images(image2, offsetx, offsety):


      """Trimming of images.

    Parameters
    ----------

    image2 : 2d numpy array (float)
        Successive ramps.(Not the first)
```

```
    offsetx: int
        Offset in x between image2 and image1

    offysety: int
        Offset in y between image2 and image1

    Returns
    -------
    IMP2 : 2d numpy array, floats
        Data array corresponding to trimmed image

    """

      i1 = j1 = 0
      i2 = image2.shape[0]
      j2 = image2.shape[1]

      IMP2= np.zeros((i2,j2))

      if offsetx >= 0 and offsety > 0 :
          IMP =  image2[(i1+offsety):i2, j1:(j2-offsetx)]
          IMP2[:(i2-offsety), (j1+offsetx):] = IMP

      elif offsetx <= 0 and offsety < 0 :
          IMP=  image2[i1:(i2+offsety), (j1-offsetx):j2]
          IMP2[(i1-offsety):,: (j2+offsetx)]=IMP

      elif offsetx < 0 and offsety >= 0 :
          IMP=  image2[(i1+offsety):i2, (j1-offsetx):j2]
          IMP2[:(i2-offsety), : (j2+offsetx)]=IMP

      elif offsetx > 0 and offsety <= 0 :
          IMP=  image2[i1:(i2+offsety), j1:(j2-offsetx)]
          IMP2[(i1-offsety):, (j1+ offsetx):]=IMP


      else :  # both offsets are zero
          IMP2 = np.copy(image2)


      return IMP2

if __name__ == "__main__":


    # define expected command-line arguments
    parser = argparse.ArgumentParser()
    parser.add_argument("input_list",
                help='"txt file with list of initial file names. Initial ramps"')

    parser.add_argument("input_offsets",
                        help='"txt file  with list of offsets between ramps"')


    parser.add_argument("--cube_with_ramps",
                        help="generate cube with ramps",
                        action="store_true")
    parser.add_argument("--trimmed_images",
                        help="generate the trimmed ramps",
                        action="store_true")

    args = parser.parse_args()


    # read list with file names
```

```
list_files = np.genfromtxt(args.input_list, dtype=[('filename_initial', '|S100')
    ])
filename_initial = list_files['filename_initial']

nfiles_initial = filename_initial.size
# nfiles_initial = number of ramps

list_offsets = np.genfromtxt(args.input_offsets,
    dtype=[('iflag', '<i8'), ('filename', '|S100'),('dark', '|S100'),
           ('offx', '<i8'), ('offy', '<i8')] )


filename = list_offsets['filename']

offx = list_offsets['offx']
offy = list_offsets['offy']

# Print the offsets between ramps
for val in zip(filename, offx, offy):
    print(val)


if offx[0] != 0 or offy[0] != 0:
    sys.exit("ERROR!!: Reference image has offsets different to zero")

naxis1 = 2048
naxis2 = 2048

image3d = np.zeros((nfiles_initial , naxis2, naxis1))

for k in range(nfiles_initial):
    image, main_header, dum = readfits(filename_initial[k])
    if image.shape != (naxis2, naxis1):
        sys.exit("ERROR!!: unexpected image dimensions")

    if k == 0:
        image3d[0,:,:] = image[:,:]
    else:
        T_image = trimming_images(image, offx[k], -offy[k] )
        image3d[k,:,:] = T_image[:,:]

median = np.median(image3d, axis=0)

#  Generating the median image of the ramps

outfile2 = re.sub('ramp1.fits\$', 'median.fits', filename_initial[0])
print("Generating the median of the ramps:\n" + outfile2)
hdu = fits.PrimaryHDU(median, main_header)
hdu.writeto(outfile2, clobber=True)

#  Generating cube with the ramps (corrected the offsets)
#  In principle we dont need generate the cube.fits

if args.cube_with_ramps:
    outfile = re.sub('ramp1.fits\$', 'cube_with_ramps.fits', filename_initial
        [0])
    print("Generating datacube with all the ramps:\n" + outfile)
    hdu = fits.PrimaryHDU(image3d, main_header)
    hdu.writeto(outfile, clobber=True)

#  Generating the trimmed images of the ramps.
#  In principle we dont need generate the trimmed images

if args.trimmed_images:
```

```
list_cube_split = []
for k in range(nfiles_initial):
    list_cube_split.append(image3d[k,:,:])
    outfile1 = re.sub('.fits\$', '_trimmed.fits', filename_initial[k])
    print("Generating␣trimmed␣images:\n" + outfile1)
    hdu = fits.PrimaryHDU(list_cube_split[k], main_header)
    hdu.writeto(outfile1, clobber=True)
```

List of Figures

1.1 Cosmic history . . . 1
1.2 Models of reionization . . . 2
1.3 CIRCE image (Left). Transmission curve of NB filter (Right) . . . 3
1.4 Readout mode of the detector . . . 4
1.5 3D-HST pointings in AEGIS (Left). Color mosaic of AEGIS-16 (Right) . . . 4

2.1 Dithering patterns obtained from the information of the headers . . . 6
2.2 OB0001: subtracted image . . . 6
2.3 The interface xnirspec (Left). Centroid fitting (Right) . . . 7
2.4 The cross-correlation technique . . . 7
2.5 OB0001: Three individual ramps . . . 8
2.6 *cleanest (REDUCEME)* interface . . . 8
2.7 Comparison between the median image and the coadded image . . . 9
2.8 Superflat i2- Superflat i1 (Left). Result i2- Result i1 (Right) . . . 10

3.1 Dithering pattern of OB0001. Coordinates obtained from the header's information are shown in red, and coordinates measured with the bright star by us are shown in blue (error bars are too small). . . . 13
3.2 Dithering pattern of OB0002 (Left) and OB0003 (Right) . . . 13
3.3 Dithering pattern of OB0004 (Left) and OB0010 (Right) . . . 14
3.4 Dithering patterns obtained by the cross-correlation technique . . . 14
3.5 HST/WFC3 image (F125W filter) of AEGIS-16 (Left). CIRCE deep image (ALBA NB filter) (Right) . . . 15
3.6 Identified objects type star . . . 20
3.7 Identified objects type galaxy . . . 20
3.8 Color-color diagram (Left). log(SFR)-log(Mass) relation (Right) . . . 21
3.9 Histogram of the distribution of the objects of AEGIS-16 . . . 22
3.10 Color-magnitude diagram of the 16 identified objects . . . 22

List of Tables

2.1 OB summary 5

3.1 Brightest star's analysis 11
3.2 Faint star's analysis 12
3.3 Seeing estimation 12
3.4 OB0001: OFFSETS BETWEEN MEDIAN IMAGES 13
3.5 Physical properties about objects type star 15
3.6 Physical properties about objects type galaxy 16
3.7 Derived properties of objects type galaxy 16